Rock Mech Rock Eng (2017) 50:967–993
DOI 10.1007/s00603-016-1141-7

ORIGINAL PAPER

Strategies for Creating Prescribed Hydraulic Fractures in Cave Mining

Q. He[1] · F. T. Suorineni[1] · J. Oh[1]

Received: 14 April 2016 / Accepted: 25 November 2016 / Published online: 2 December 2016

Abstract The cave mining method was traditionally applied to massive low-grade, weak orebodies at shallow depths (less than 500 m) that favour cave propagation under gravity. Currently, this method is being applied to stronger orebodies and is taking place at depths of up to 2000 m below the surface. To ensure continuous cave propagation, preconditioning of the orebody is essential in this latter caving environment to improve rock mass caveability and to decrease fragmentation sizes. Hydraulic fracturing was initiated in the oil industry and is now being used in the cave mining industry as a preconditioning method and for stalled caves reactivation. A limitation of conventional hydraulic fracturing in the cave mining industry is that the hydraulic fracture orientation is uncontrollable and is dictated by the minimum in situ stress orientation. The preconditioning effectiveness of orientation-uncontrollable hydraulic fractures is limited in some geotechnical conditions, and the concept of creating orientation-controllable hydraulic fractures, here termed prescribed hydraulic fractures, is proposed to fill this gap. In this paper, the feasibility of the proposed approaches to creating prescribed hydraulic fractures is presented based on previous studies and numerical modelling. The numerical modelling code reliability in simulating the hydraulic fracture propagation and reorientation process was validated by comparing with laboratory results in the reported literature. In addition, the sensitivity of the prescribed hydraulic fracturing to the in situ stress condition and rock mass properties is examined.

✉ F. T. Suorineni
f.suorineni@unsw.edu.au

[1] School of Mining Engineering, Faculty of Engineering, UNSW Australia, Sydney, NSW 2052, Australia

Keywords Prescribed hydraulic fracturing · Hydraulic fracture reorientation · Numerical modelling · Block caving

List of symbols

σ_1	The maximum principal stress (MPa)
σ_2	The intermediate principal stress (MPa)
σ_3	The minimum principal stress (MPa)
σ_{hmax}	The maximum horizontal principal stress (MPa)
σ_{hmin}	The minimum horizontal principal stress (MPa)
σ_X	Fracture-induced stress in the far-field intermediate principal stress direction (MPa)
σ_Z	Fracture-induced stress in the far-field minimum principal stress direction (MPa)
σ'_h	Superimposed stress near the fracture surface in the far-field intermediate principal stress direction (MPa)
σ'_v	Superimposed stress near the fracture surface in the far-field minimum principal stress direction (MPa)
σ_n	The net pressure (MPa)
σ_d	The differential stress between the intermediate principal stress and the minimum principal stress (MPa)
E	Young's modulus (MPa)
m	Homogeneity Index
K_{Ic}	Rock fracture toughness (Pa $m^{1/2}$)
L_d	The fracture spacing (m)
L_h	The fracture half-length (m)
L_s	The shadow-free zone length (m)
r	The fracture radius (m)
u	The material property assigned to a given element
u_0	The mean value of the material property
v	The Poisson's ratio
$\mathcal{D}$	The dimensionless differential stress
$\mathcal{S}$	The dimensionless confining stress

$\mathcal{W}$ The dimensionless propped fracture width

1 Introduction

Hydraulic fracturing had its first commercial application in 1949 (Clark 1949). This technique has been commonly used in the oil and gas industries to enhance reservoir permeability by creating artificial fractures in the reservoir formation. Recently, hydraulic fracturing has been introduced into the mining industry with the purposes of improving coal seam permeability in the coal mining industry (Puri et al. 1991a, b; Zhai et al. 2012), inducing hard roof caving in the coal mining industry (Chernov 1982; Jeffrey and Mills 2000; Jeffrey et al. 2001; Fan et al. 2012; He et al. 2012; Lekontsev and Sazhin 2014), enhancing top coal caveability for longwall top coal caving (Huang et al. 2011, 2015), and reactivating caving and/or preconditioning the orebody in the cave mining industry (Jeffrey 2000; Van As and Jeffrey 2000a, b; van As et al. 2004; Catalan et al. 2012).

When hydraulic fracturing is used in cave mining for preconditioning, boreholes are drilled from the surface or subsurface excavations into the orebody to create multiple transverse hydraulic fractures (HFs) along each borehole. These artificial fractures aim to improve rock mass caveability and reduce fragmentation sizes, which are critical to the successful application of the cave mining method. The hydraulically fractured orebody is expected to cave under gravity after undercuting to a specific size based on the orebody quality normally determined by the Laubscher rules (Laubscher 1994).

The cave mining method offers the lowest operating cost and the most productive mining system compared with any other underground miming system provided the rock mass condition is suitable. Chitombo (2010) stated that this method was traditionally applied to weak orebodies and is now being applied to stronger orebodies with targeted caving heights of 500–550 m.

Previous studies on cave mining hydraulic fracturing are focused on field applications, HF growth measurement, and the interaction between HFs and natural fractures (NFs). The cave inducement practice at Northparkes Mine shows hydraulic fracturing can improve rock mass caveability to reactivate the caving of a stalled cave back (Van As and Jeffrey 2000a, b). The experience at Salvador Mine indicates the preconditioned rock mass quality is decreased significantly as inferred from the P-wave velocity change from 2 to 4 ms over a 60-m distance and the spacing between HFs has a strong effect on the fragmentation size (Chacon et al. 2004).

Monitoring boreholes often provides direct measurement of HF size and its propagation rate (van As et al. 2004). Tiltmeter monitoring is an effective way to estimate the HF orientation and size (van As et al. 2004). Stress change monitoring is also used to observe HF orientation and opening mode (Chacon et al. 2004; Mills et al. 2004). The effect of micro-seismic monitoring on HF performance is mine site-dependent, and continuous data recording at high frequency improves its accuracy (Jeffrey et al. 2009; Joubert 2010) in characterizing the HF.

Mine through mapping is the only direct way to investigate the HF trajectory and its interaction with NFs (van As and Jeffrey 2002; Jeffrey et al. 2009). In the field, the HF radius may be shorter than its theoretical prediction due to its interaction with NFs. This process highly depends on the in situ stress condition and the NF orientation (He et al. 2015). Generally, HFs tend to cross NFs at about 90° interaction angles and grow into NFs at acute interaction angles (van As and Jeffrey 2002). Infillings in NFs are helpful in increasing NF shear strength and decreasing NF permeability so that HFs can cross NFs without offsetting (Catalan et al. 2012). Shear zones that usually have weaker shear strength and higher permeability (compared with NFs) have significant influence on HF propagation and act as barriers that result in asymmetrical HF propagation.

Theoretically, the HF propagation path is controlled by and is perpendicular to the minimum principal stress (σ_3) orientation (Hubbert and Willis 1972). From the above review, current hydraulic fracturing operations are designed based on this principle to create HFs having fixed orientations. These studies hypothesize that the orebody could be well preconditioned as long as numbers of HFs are created joint frequency. However, this assumption might be debatable. To achieve effective preconditioning, a blocky hydraulically fractured orebody is necessary and desirable, which implies the relative orientations of the created HFs to the existing NFs are important.

The in situ σ_3 orientation at most caving mine sites in Australia is vertical and favours creation of horizontal HFs. He et al. (2016a) noticed that the preconditioning efficiency in this in situ stress condition might be ineffective as shown in Fig. 1a, where the orebody contains no dominant NFs, and Fig. 1b, where the orebody is dominated by horizontal NFs. In either of these scenarios, no blocky orebody is created. Therefore, HFs with controllable orientations are required so that effective preconditioning can be achieved in various geotechnical conditions (Fig. 1c).

In the case of an orebody or rock mass containing fracture or fractures, the presence of the fracture or fractures results in the stress state in the region around the fracture surfaces to be altered as a result of the superimposition of the in situ stress state and the fracture-induced stress state. The fracture-induced stress vector at each point in the near-fracture region can be decomposed into two sub-vectors as σ_Z, which is the stress vector in the vertical

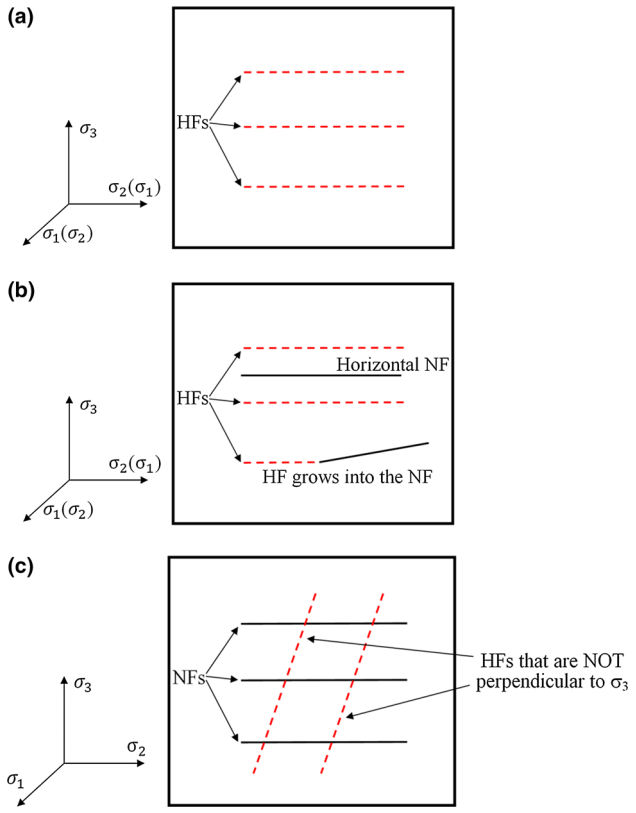

Fig. 1 Relative efficiency of traditional hydraulic fracturing and prescribed hydraulic fracturing (He et al. 2016a): **a** traditional hydraulic fracturing in an orebody without dominant NFs; **b** traditional hydraulic fracturing in an orebody containing horizontal NFs; **c** a blocky orebody is created by prescribed hydraulic fracturing

direction, and σ_X, the stress vector in the horizontal direction. If the difference between the fracture-induced stresses σ_Z and σ_X exceeds the difference between the initial far-field stresses σ_2 and σ_3, the minimum principal stress orientation in the near-fracture region will rotate by 90° as the component of the superimposed stress vector in the vertical direction, σ'_v, at each point in this region is larger than that in the horizontal direction, σ'_h. This phenomenon described here is called the stress shadow effect (Elbel and Mack 1993; Siebrits et al. 1998; Wright and Weijers 2001).

To fill the gap of creating HFs with controllable orientations so that effective preconditioning can be achieved, He et al. (2016a) proposed the concept of prescribed hydraulic fracturing (Fig. 1c) and concluded prescribed hydraulic fractures (PHFs) with controllable orientations could be created if the stress shadow effect is properly utilized and combined with directional hydraulic fracturing (DHF) practice. Further details of prescribed hydraulic fracturing can be found in (He et al. 2016a).

In this paper, the feasibility of prescribed hydraulic fracturing is studied by numerical modelling. The numerical code used in this study is called the realistic failure process analysis (RFPA) 3D flow model, and its ability to simulate hydraulic fracturing is validated by comparing its simulation results with laboratory results. The validated code is then used to simulate prescribed hydraulic fracturing in a laboratory-scale model. In addition, the sensitivity of prescribed hydraulic fracturing to the in situ stress condition and rock mass properties is investigated.

The rest of the paper is organized as follows. Section 2 briefly describes the two approaches proposed in (He et al. 2016a) for creating PHFs. Section 3 discusses the feasibility of prescribed hydraulic fracturing based on a summary of previous studies on the stress shadow effect and DHF methodology. Section 4 provides the results in two companion papers in which the reliability of RFPA3D is proved. In Sect. 5, the validated code is then applied to investigating the feasibility of prescribed hydraulic fracturing and its sensitivity to in situ stress conditions and rock mass properties. Finally, some conclusions are provided in Sect. 6.

2 Approaches to Creating Prescribed Hydraulic Fractures in Cave Mining

To create PHFs as described in Fig. 1c, a novelty in HF reorientation against its theoretically predicted direction is needed. Previous studies reveal that the HF propagation path can be reoriented by either the stress shadow effect that results in the local stress change (Elbel and Mack 1993; Siebrits et al. 1998; Wright and Weijers 2001) or an oriented initial weakness that controls the HF initiation direction (Fan et al. 2012; He et al. 2012, 2016c).

The stress shadow effect is related to the stress reversal around a fracture having a certain width. Figure 2a shows a horizontal fracture intersecting the borehole with the in situ σ_3 orientation assumed to be vertical. This fracture can be either a newly created HF or a reopened NF during the hydraulic fracturing operation. The residual fluid and proppants (if proppants are used) inside of the fracture are under compression due to the in situ stress and the deformation of the rock mass to enable the fracture retain an open width. In fracture mechanics (Anderson and Anderson 2005), the fracture in Fig. 2a is described as a tensile fracture, which is formed by the tensile stresses applied perpendicularly to the fracture surfaces.

Figure 2b illustrates the basic idea of DHF. In cave mining, the HF is transverse (i.e. perpendicular to the borehole) and has a radial shape. In field applications, the cutting machine is used to cut an initial notch around the borehole wall as an artificial weakness for the HF to initiate (Catalan et al. 2012). If the notch orientation is not aligned with the HF preferred propagation direction, the HF will undergo a gradual reorientation process until it finally

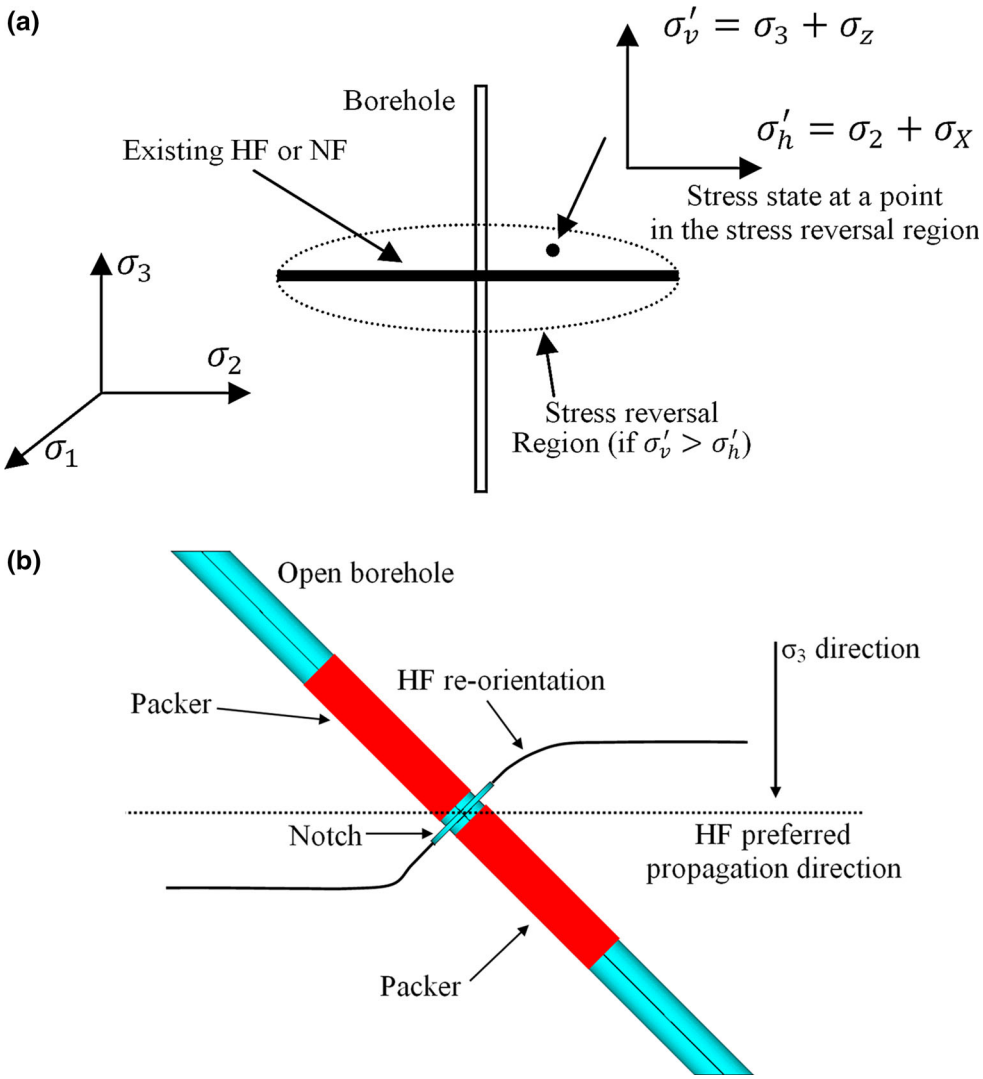

Fig. 2 Two mechanisms causing HF reorientation: **a** the stress shadow effect that results in the local stress change (Roussel and Sharma 2011a); **b** directional hydraulic fracturing that controls the HF initiation direction (He et al. 2016c)

propagates perpendicularly to the far-field σ_3 orientation (He et al. 2016c). The two approaches are described in the following sections.

2.1 Approach One

Figure 3 illustrates the basic idea of the first approach (He et al. 2016a) for creating PHFs. Two fractures are pre-located before prescribed hydraulic fracturing. These pre-located fractures can be produced by prior hydraulic fracturing or are NFs. The pre-located fractures are propped to enhance the induced stress shadow effect, so that the stress reversal regions around the pre-located fractures overlap each other and occupy the whole space between the pre-located fractures as shown in Fig. 3a. The local σ_3 orientation between the pre-located fractures now becomes horizontal and is aligned with the far-field σ_2 orientation.

The DHF practice is performed in the stress reversal region as shown in Fig. 3b. An initial notch is cut around the borehole wall at the middle of the pre-located fractures as an artificial weakness for the HF to initiate. The HF is expected to initiate transversely along the notch orientation and then reorientate its path to propagate vertically towards the pre-located fractures. The overall PHF orientation in Approach One is parallel to the far-field σ_3 orientation as shown in Fig. 3b.

2.2 Approach Two

Figure 4 illustrates the basic idea of the second approach. Different from the stress state in Approach One, the stress shadows of the pre-located fractures in Approach Two do not overlap each other, and hence a stress shadow-free zone remains between the pre-located fractures as shown in

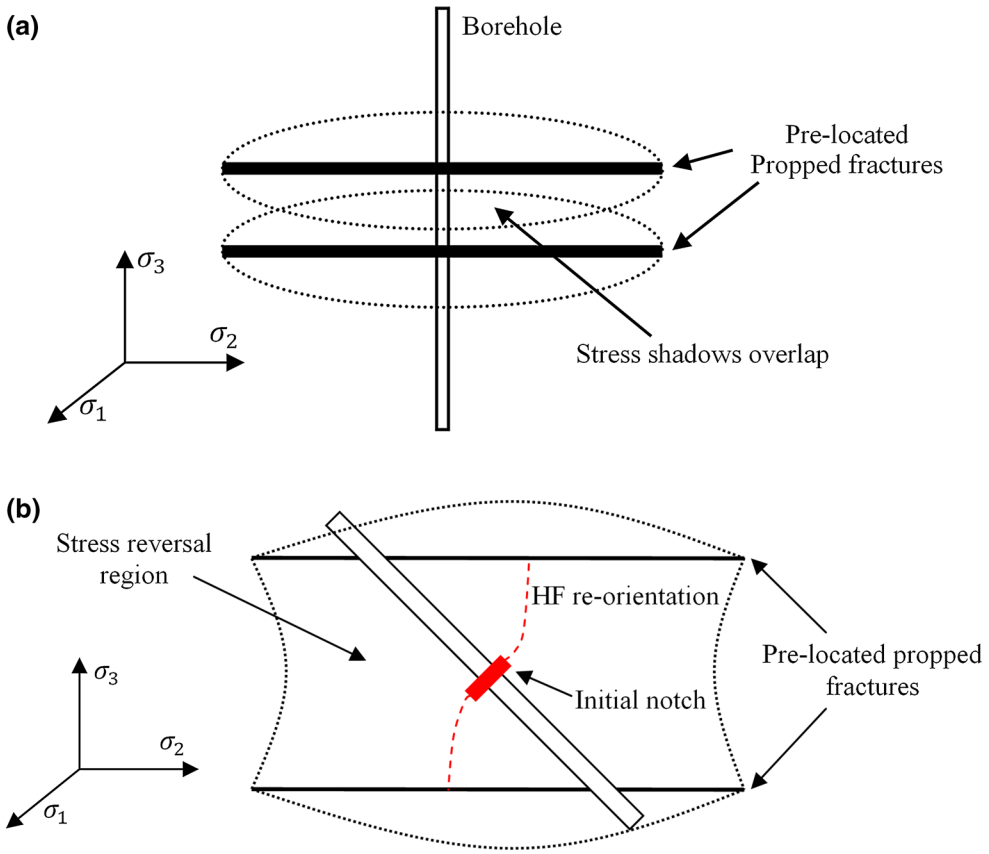

Fig. 3 First approach to creating PHFs (He et al. 2016a): **a** stress shadows of the pre-located fractures overlap each other to form a stress reversal region that occupies the whole space between the pre-located fractures; **b** the HF initiates in the stress reversal region and reorientates vertically towards the pre-located fractures to form a PHF that is parallel to the far-filed σ_3 orientation

Fig. 4a. In the stress shadow-free zone, the local σ_3 orientation is not rotated and is still aligned with the far-field σ_3 orientation.

In cave mining, water is often used in the hydraulic fracturing process without proppants, which does not favour stress shadows overlap between the pre-located fractures. The low viscosity of water results in a narrower initial fracture width, as well as a limited stress shadow effect, compared with that when more viscous fluid is used as in the oil and gas industries. However, although the local σ_3 orientation in the stress shadow-free zone is not altered, the differential stress in this zone is expected to decrease dramatically due to the induced stresses around the pre-located fractures. This favours the utilization of DHF to prescribe the HF propagation direction.

As shown in Fig. 4b, the HF is expected to experience a secondary reorientation process and propagate towards the pre-located fractures as long as the HF propagates long enough to enter the stress reversal regions around the pre-located fractures. In this case, the overall PHF orientation in Approach Two is oblique to and not perpendicular to the far-field σ_3 orientation as shown in Fig. 4b.

3 Previous Studies on the Stress Shadow Effect and Directional Hydraulic Fracturing

In this section, the feasibility of prescribed hydraulic fracturing is discussed based on the review of previous studies on the stress shadow effect and directional hydraulic fracturing.

3.1 Stress Shadow Effect

Studies on the stress shadow effect were initiated in the shale gas industry with the purposes of avoiding the interaction between multiple HFs and ensuring their parallel propagation. This subject has been widely studied by numerical modelling by various researchers (Olson 2008; Cheng 2009; Roussel and Sharma 2011a, b; Manchanda and Sharma 2012; Morrill and Miskimins 2012; Rafiee et al. 2012; Roussel et al. 2012; Wu et al. 2012; Geilikman et al. 2013; Xu and Wong 2013). These studies reveal that the extent of the stress reversal region is determined by many factors that include the in situ differential stress, rock mass properties, fracture dimensions, the pre-located fracture width, and the fracture spacing. He et al. (2016b)

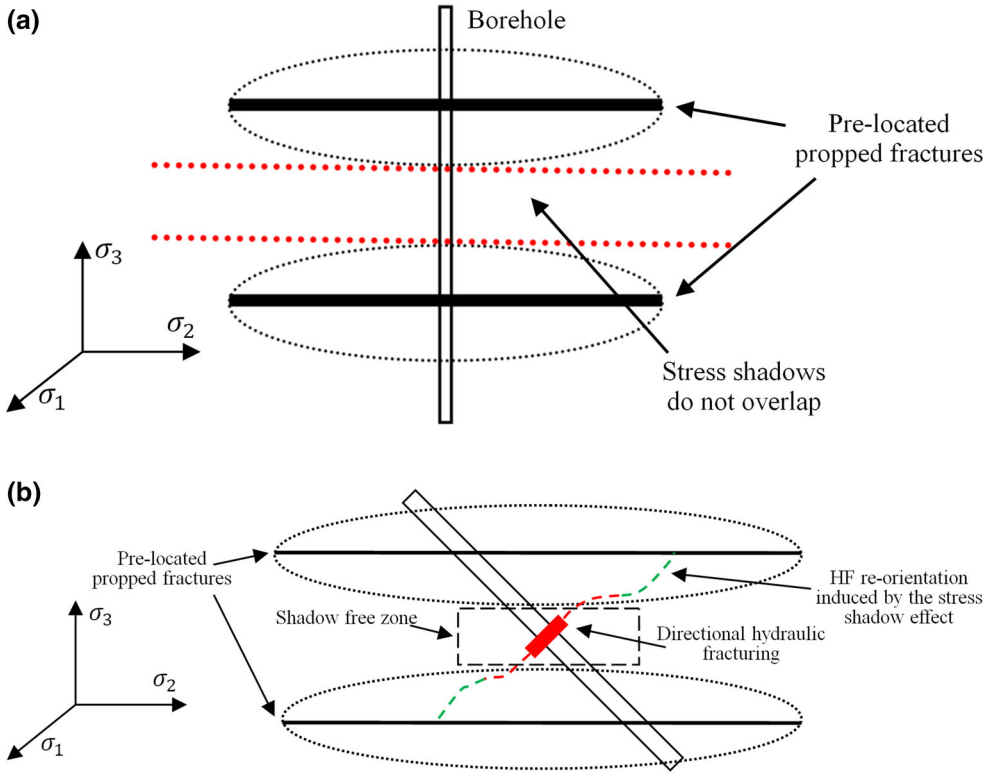

Fig. 4 Second approach to creating PHFs (He et al. 2016a): **a** stress shadows of the pre-located fractures do not overlap each other and hence a shadow-free zone remains between the pre-located fractures; **b** the HF initiates in the shadow-free zone by DHF and undergoes a secondary reorientation process induced by the pre-located fractures to form a PHF that is oblique to the far-field σ_3 orientation

investigated the interaction among closely located fractures (1–2.5 m) in cave mining and concluded that not only the differential stress between σ_3 and σ_2 but also the differential stress between σ_3 and σ_1 influences the HF reorientation process and the traditional material homogeneity assumption used in previous studies might be debatable in predicting the HF reorientation trajectory as the HF may have a long reorientation distance in a more heterogeneous rock mass.

The HF trajectory could deviate from its theoretical prediction due to the stress shadow effect around a single fracture or the stress shadow effect between fractures. The latter phenomenon is of much interest in this study for its utilization in the proposed approaches depicted in Figs. 3b and 4b.

Roussel and Sharma (2011a) studied the extent of stress reversal regions around a single fracture and between two pre-located fractures with a three-dimensional numerical model based on the geotechnical condition in the Barnett Shale. The selected modelling scenarios and their results are provided in Table 1, where σ_n is the fracture net pressure (i.e. the difference between the fracture internal pressure induced by the proppant and the in situ stress applied perpendicularly to the fracture surfaces), σ_d is the differential stress between the far-field horizontal principal stresses, L_d is the fracture spacing, L_h is the fracture half-length, and L_s is the stress shadow-free zone length. Figure 5 shows the maximum principal stress (σ_1) distribution in each modelling case. In each subfigure of Fig. 5, a plan view is provided. The borehole is horizontal and parallel to the far-field σ_3 orientation. The HF is transverse, and its orientation is perpendicular to the far-field σ_3 orientation.

The σ_n/σ_d ratio in each modelling case in Table 1 was constant (0.49), and the HF had a half-length of 152.4 m (500 ft.). In Case 1, a single HF with a propped width of 4 mm was simulated. Figure 5a shows the σ_1 distribution in Case 1. Due to the fracture-induced stress, a stress reversal region occurs around the fracture surface to the extent of about 45.7 m (150 ft.). In this region, the σ_1 orientation is rotated by 90° and becomes perpendicular to the fracture orientation. The simulation result confirms the basic idea of the stress shadow effect illustrated in Fig. 2a that results in the local stress change.

In Cases 2–4, two pre-located fractures were simulated, and the L_d/L_h ratio was increased from 1.20 to 1.40 with a constant L_h value. Figure 5b shows the σ_1 distribution in Case 2 where the stress shadows of the two pre-located fractures overlap each other. As shown in Fig. 5b, the σ_1 orientation between the pre-located fractures becomes aligned with the far-field σ_3 orientation, which implies a

Table 1 Modelling results in (Roussel and Sharma 2011a) where the stress reversal regions around a single fracture and between two pre-located fractures are studied

Modelling result	Net pressure σ_n (MPa)	Differential stress σ_d (MPa)	σ_n/σ_d	Fracture distance L_d (m)	Fracture half-length L_h (m)	L_d/L_h	Shadow-free zone length L_s (m)	L_s/L_d
1	0.34	0.69	0.49	–	152.4	–	–	–
2	0.34	0.69	0.49	182.88	152.4	1.20	–	–
3	0.34	0.69	0.49	198.12	152.4	1.30	6.10	0.03
4	0.34	0.69	0.49	213.36	152.4	1.40	67.06	0.31

new HF initiated in this stress reversal region will propagate parallel to rather than perpendicularly to the far-field σ_3 orientation. The result in Case 2 proves the required stress state in Approach One as depicted in Fig. 3a can be created if the pre-located fractures are placed close enough to have their stress shadows overlapping each other.

In Cases 3–4, with the increase in the fracture spacing, a stress shadow-free zone occurred between the pre-located fractures. The stress shadow-free zone tended to become wider with a higher L_d/L_h ratio as indicated by the results in Table 1. Figure 5c shows the σ_1 distribution in Case 4. In the stress shadow-free zone, the σ_1 orientation is not altered by the fracture-induced stresses and is still consistent with the in situ stress condition. This implies that to create PHFs in the shadow-free zone, DHF practice is necessary to reorientate the HF propagation path as illustrated in Figs. 2b and 4b.

The modelling results in Table 1 also indicate that to create a stress reversal zone that occupies the whole space between pre-located fractures as required in Approach One, the net pressure does not need to be higher than the initial differential stress provided the L_d/L_h ratio is sufficiently low (Case 2). With the increase in the L_d/L_h ratio, a shadow-free zone occurs between pre-located fractures as that in Approach Two. The shadow-free zone length and the L_s/L_d ratio are very sensitive to the change in the L_d/L_h ratio (Case 3 and Case 4). To create the required stress state in either Approach One or Approach Two, the fracture spacing is on the order of the fracture half-length (Case 2–4). This implies if two fractures having radii of 10 m are pre-located and propped, the PHF vertical length might be up to 13 m.

Rafiee et al. (2012) used the boundary element method to investigate the induced stress change between two pre-located fractures. The modelling results are provided in Table 2. From Cases 1–4, the σ_n/σ_d ratio was constant (0.8), and the L_d/L_h ratio was increased from 0.50 to 1.25. From Case 5 to Case 8, the L_d/L_h ratio was constant (1.00), and the σ_n/σ_d ratio was increased from 0.53 to 1.33. The modelling results in Table 2 indicate the σ_n/σ_d ratio is another key factor that determines the stress state between pre-located fractures. A high σ_n/σ_d ratio and a low L_d/L_h ratio favour the elimination of the shadow-free zone (Case 1, Case 2, Case 7, and Case 8). In the modelling case where shadow-free zone occurs (Case 3, Case 4, Case 5, and Case 6), although the σ_3 orientation in this shadow-free zone is still aligned with the far-field σ_3 orientation, the local differential stress decreases dramatically due to the fracture-induced stresses. This low local differential stress favours the utilization of DHF to prescribe the HF propagation direction as depicted in Approach Two.

The above studies are focused on the calculation of the stress state between pre-located fractures or around a pre-located fracture and assume the HF reorientation trajectory is determined by the calculated stress state. Bunger et al. (2011, 2012; Kear et al. 2013) carried out a series of studies on the interaction among closely located fractures in cave mining. From the investigation of the HF reorientation trajectory with a two-dimensional numerical model, Bunger et al. (2012) drew a different conclusion that showed the newly created HF could reorientate towards the pre-located fracture provided the reopening or the sliding of the pre-located fracture occurred due to the induced stress around the newly created HF tip. Dimensional analysis (Barenblatt 1996) was applied to Bunger et al.'s study, and some of the obtained dimensionless groups are listed in Table 3, where K_{Ic} is the rock fracture toughness, w is the fracture maximum propped width, E is the Young's modulus, and ν is the Poisson's ratio. These dimensionless groups indicate rock fracture toughness may have important influence on HF reorientation. High rock fracture toughness may weaken the influence of the differential stress (dimensionless group $\mathcal{D}$) and the induced stress shadow effect (dimensionless groups $\mathcal{S}$ and $\mathcal{W}$) on the HF reorientation process.

3.2 Directional Hydraulic Fracturing and Hydraulic Fracture Reorientation from Oriented Perforations

DHF is used in an open borehole to prescribe the HF initiation location and its orientation by cutting an initial notch around the borehole wall as shown in Fig. 2b. Although this technique has wide applications in the

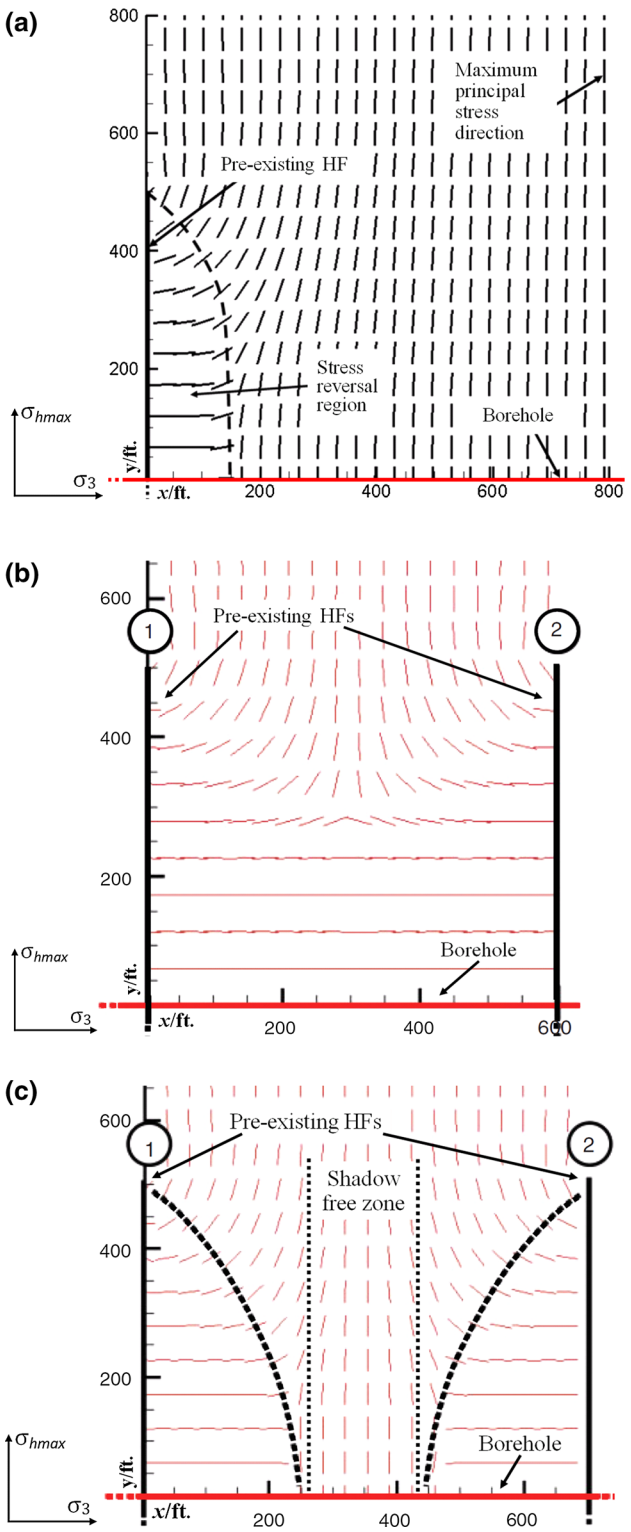

◀**Fig. 5** Maximum principal stress (σ_1) distributions around a single fracture and between two pre-located fractures (Roussel and Sharma 2011a): **a** the σ_1 distribution around a single fracture, which shows a stress reversal region occurs around the fracture surface; **b** the σ_1 distribution between two pre-located fractures, which shows the stress shadows overlap each other and the stress reversal region occupies the whole space between the pre-located fractures; **c** the σ_1 distribution between two pre-located fractures, which shows the stress shadows do not overlap each other and a shadow-free zone remains between the pre-located fractures

mining industry (Chernov 1982; Chernov and Kyu 1996; Chernov et al. 1997; Jeffrey and Mills 2000; Lekontsev and Sazhin 2008; Fan et al. 2012; He et al. 2012; Jeffrey et al. 2013; Lekontsev and Sazhin 2014; Huang et al. 2015), few studies have been carried out to investigate the HF reorientation process from an oriented initial notch. He et al. (2016c) simulated directional HFs with a three-dimensional numerical model and found that compared with the differential stress between σ_3 and σ_1, the differential stress between σ_3 and σ_2 dominates the HF reorientation process if the borehole is assumed to lie on the σ_2–σ_3 plane. The HF tends to have a longer reorientation distance in more heterogeneous rock masses and reorientate abruptly in more homogeneous rock masses.

HF reorientation from oriented perforations has been widely studied in laboratory experiments (Daneshy 1971, 1973a, b; Behrmann and Elbel 1991; Weijers and De Pater 1992; Abass et al. 1994, 1996; Chen et al. 2010) and by numerical modelling (Guangqing and Mian 2009; Sepehri 2014; Sepehri et al. 2015). From experimental studies, Behrmann and Elbel (1991) and Abass et al. (1994) observed HF reorientation from oriented perforations occurs within one or two borehole diameters. This implies the HF reorientation distance from an oriented initial notch should be no more than 20 cm (the borehole diameter in cave mining is about 10 cm), and Approach Two depicted in Fig. 4b may not be applicable in field applications. However, it should be noted that the experimental environments in Behrmann et al.'s study and Abass et al.'s study are very different from the potential stress state and rock conditions in Approach Two. Tables 4 and 5 provide the rock properties and the stress states in Behrmann et al.'s study and Abass et al.'s study, respectively. The rock samples used in these studies were sandstone and hydrostone that represented rock conditions in the oil industry and had much lower strength than that in cave

Table 2 Modelling results in (Rafiee et al. 2012) where the induced stress change between two pre-located fractures is studied

Modelling result	Net pressure σ_n (MPa)	Differential stress σ_d (MPa)	σ_n/σ_d	Fracture distance L_d (m)	Fracture half-length L_h (m)	L_d/L_h	Induced stress change (MPa)
1	2.07	2.59	0.80	60.96	121.92	0.50	≥2.59
2	2.07	2.59	0.80	91.44	121.92	0.75	≥2.59
3	2.07	2.59	0.80	121.92	121.92	1.00	2.07–2.41
4	2.07	2.59	0.80	152.40	121.92	1.25	1.72–2.07
5	1.38	2.59	0.53	121.92	121.92	1.00	1.38–1.72
6	2.07	2.59	0.80	121.92	121.92	1.00	2.07–2.41
7	2.76	2.59	1.07	121.92	121.92	1.00	≥2.59
8	3.45	2.59	1.33	121.92	121.92	1.00	≥2.59

Table 3 Selected dimensionless groups in (Bunger et al. 2012) that show the potential correlation between the physical quantities

Dimensionless differential stress	Dimensionless confining stress	Dimensionless propped opening	Dimensionless fracture radius
$\mathcal{D} = \frac{\sigma_d\sqrt{L_d}}{K_{Ic}}$	$\mathcal{S} = \frac{\sigma_3\sqrt{L_d}}{K_{Ic}}$	$\mathcal{W} = \frac{wE\sqrt{L_d}}{K_{Ic}L_h(1-\nu^2)}$	$\frac{L_h}{L_d}$

mining. The differential stress magnitude was about 7.5 MPa, and triaxial stress states were simulated in these studies. Table 6 provides rock conditions and stress states at some caving mine sites in Australia. Rocks at these mine sites are more competent, which may weaken the influence of the differential stress on HF reorientation according to Bunger et al.'s assumption in dimensional analysis (Bunger et al. 2012). The in situ differential stress magnitudes at the mine sites range from 2.9 to 7.0 MPa, and the local differential stress magnitudes in the potential shadow-free zones depicted in Approach Two should decrease significantly due to the fracture-induced stresses as proved in Table 2.

Table 4 Rock conditions and stress states in Behrmann et al.'s experiment (Behrmann and Elbel 1991)

Rock type	Saturated strength	$\sigma_2 - \sigma_3$ (MPa)
Torrey sandstone	About 41.37 MPa	7.45
Gold sandstone	About 27.60 MPa	7.45

Table 5 Rock properties and the stress state in Abass et al.'s experiment (Abass et al. 1994, 1996)

Rock type	Young's modulus	UCS	$\sigma_2 - \sigma_3$
Hydrostone	14.3 GPa	55.4 MPa	7.58 MPa

Table 6 Rock conditions and stress states at some caving mine sites in Australia (Van As and Jeffrey 2000a, b; Jeffrey et al. 2009; Catalan et al. 2012; Kaiser et al. 2013)

Mine site	Young's modulus (GPa)	UCS (MPa)	$\sigma_2 - \sigma_3$ (MPa)
E26, Northparkes	60.0	120.0	2.9
E48, Northparkes	50.8	93.8	6.0
Cadia East	67.0	133.0	7.0

3.3 Discussion

From previous studies on the stress shadow effect, DHF, and HF reorientation from oriented perforations, the following conclusions are drawn. The stress state between two pre-located fractures highly depends on the σ_n/σ_d ratio (if σ_3 is assumed to be horizontal), which represents the relative net pressure to the in situ differential stress, and the L_d/L_h ratio, which represents the relative fracture spacing to the fracture half-length. To either create a stress reversal region that occupies the whole space between the pre-located fractures in Approach One (Fig. 3a) or a small shadow-free zone in Approach Two (Fig. 4a), the net pressure does not need to be higher than the in situ differential stress as long as the pre-located fractures are placed closely enough (Tables 1, 2). For fixed propped fracture dimensions (i.e. the fracture half-length and the propped fracture width), the induced stress shadow effect is stronger in rock masses with higher Young's modulus (Manchanda and Sharma 2012; Roussel et al. 2012). High rock fracture toughness may weaken the influence of the differential stress on HF reorientation, which offers the HF a longer reorientation distance from an oriented initial notch (Bunger et al. 2012). The PHF may propagate towards a pre-located fracture due to its interaction with this fracture. The PHF tends to propagate towards a pre-located fracture if the opening or the sliding of the pre-located fracture occurs (Bunger et al. 2012). The inference that the HF

reorientation distance from an oriented weakness is within one to two borehole diameters (Behrmann and Elbel 1991; Abass et al. 1994) may not be applicable in estimating the HF reorientation distance induced by DHF in Approach Two. The reason is that, compared with the experimental environments where the above inference was made, the rock in cave mining has a stronger quality (Table 6) and the shadow-free zone in Approach Two may have a much lower differential stress (Table 2).

To realize Approach One, a stress reversal region that occupies the whole space between the pre-located fractures is required. Water is normally used in cave mining hydraulic fracturing, and the HF radius is about 30 m (Bunger et al. 2011). Mills et al. (2004) performed stress change monitoring at Northparkes Mines and observed that the induced stress change recorded from monitoring instruments located 14–48 m above the HF was from 0.5 to 1.4 MPa. This stress change was induced by a single fracture, and the monitoring distance was much longer than the potential fracture spacing in Approach One. Currently, the distance between multiple HFs in cave mining ranges from 1 to 2.5 m (Bunger et al. 2011). This is to ensure that the HF propagates parallel to each other without the stress disturbance from closely located fractures.

In Approach One, the disadvantage of the stress shadow effect is turned into an advantage that induces the required HF reorientation. A 5–10-m fracture spacing should be reasonable. A fracture spacing in this range leads to a low L_d/L_h ratio that favours the utilization of the stress shadow effect and tends to achieve small fragmentation sizes. In field applications, a numerical simulation could be performed to calculate the stress distribution between pre-located fractures to ensure that the stress reversal region occupies the whole space between the pre-located fractures under the given operation parameters, such as the pre-located fracture radius, the propped fracture width, and the fracture spacing.

In Approach Two, a shadow-free zone remains between the pre-located fractures. This approach may be more commonly used in cave mining for the following reasons. The fracture width, as well as the induced stress shadow effect, is limited when water is used as fracturing fluid, and some mine sites may have a high in situ differential stress, such as that at Cadia East Mine (7.0 MPa). In field applications, proppants may not distribute uniformly in pre-located fractures, which decreases the net pressure magnitude and the σ_n/σ_d ratio. The pre-located fracture may have a shorter radius compared with its theoretical prediction due to its interaction with NFs, which results in a higher L_d/L_h ratio.

To realize Approach Two, a long HF reorientation distance induced by DHF is required. He et al. (2016c) simulated the HF trajectory from a prescribed initial notch in a hydrostatic stress state and observed that the HF propagates along the notch direction within a long distance and may have a little deviation from this path due to rock mass heterogeneity. This implies the HF tends to propagate along the prescribed notch orientation in a low differential stress state, such as that in the shadow-free zone in Approach Two.

In the following sections, the speculation on the feasibility of prescribed hydraulic fracturing will be verified by numerical modelling. The model's ability to simulate hydraulic fracturing was validated in two companion papers. In the next section, the results in these studies will be presented.

4 Numerical Code and Model Validation

Previous studies on hydraulic fracturing simulation are focused on the prediction of fluid pressure, the fracture width, the fracture length (or radius), and the interaction between HFs and NFs (Adachi et al. 2007; Rogers et al. 2011; Brzovic et al. 2015; He et al. 2015; Katsaga et al. 2015). In these studies, the HF is normally assumed to have a regular planar or radial shape. In this study, the priority of hydraulic fracturing simulation is the prediction of the HF reorientation trajectory. The HF in this situation has an irregular shape.

The selected modelling tool, the RFPA 3D flow model, is based on the basic realistic failure process analysis model (Tang 1997; Tang et al. 1998) and the flow-stress-damage model (Tang et al. 2002). Its mechanism was described in detail in (Tang et al. 2002; Li et al. 2012), and its two-dimensional version has a number of applications in simulating hydraulic fracturing in heterogeneous rock masses (Tang et al. 2003; Yang et al. 2003, 2004; Li et al. 2005; Wang et al. 2009, 2013; Men et al. 2013).

He et al. (2016c) examined RFPA3D's ability to simulate HF reorientation from oriented perforations by comparing with the results of Abass et al.'s laboratory experiment (Abass et al. 1994), and He et al. (2016b) proved RFPA3D is able to predict HF reorientation induced by the stress shadow effect by comparing with the results of Bunger et al.'s laboratory experiment (Bunger et al. 2011). These two HF reorientation mechanisms are the basic components of the proposed approaches to creating PHFs. In this section, the validation results are presented to demonstrate the HF reorientation trajectories simulated by RFPA3D can lead to realistic results.

4.1 Hydraulic Fracture Reorientation from Orientated Initial Weaknesses

4.1.1 Abass et al.'s Laboratory Experiment

Up to now, no laboratory experiment has been performed to investigate HF reorientation caused by DHF. Abass et al. (1994) experimentally studied the HF reorientation process from oriented perforations. The perforation technique is commonly used in a cased borehole and can cause planar HF reorientation if the perforation orientation is not aligned with the HF preferred propagation plane. HF reorientation from an oriented initial notch (i.e. DHF) and HF reorientation from oriented perforations are technically different, but these phenomena are essentially similar to each other because both of them are HF reorientation from orientated initial weaknesses. The HF reorientation trajectories in Abass et al.'s experiment were well recorded and thus provide excellent grounds for model validation.

The rock samples used in Abass et al.'s experiment were blocks of hydrostones with dimensions of 152.4 mm × 152.4 mm × 254 mm. A cased vertical borehole (14.5 mm in inner diameter and 19.0 mm in outer diameter) was perforated (with 10 perforations at 180° phasing) along a 50.8 mm section around the borehole centre. The perforation depth and the perforation diameter were 12.7 mm and 3.4 mm, respectively. 90-weight gear oil, whose viscosity is 1.18 Pa•s, was used as the fracturing fluid and was injected at a flow rate of 5 e^{-7} m^3/s. A trial stress state was applied to each sample, and the stress magnitudes were $\sigma_v = 20.7$ MPa, $\sigma_{hmax} = 17.2$ MPa, and $\sigma_{hmin} = 9.7$ MPa. The sample properties are listed in Table 7. Figure 6 presents the plane views of the planar HF reorientation trajectories with different perforation angles in Abass et al.'s study. The two-dimensional section plane used to present the three-dimensional HF trajectory is illustrated in Fig. 7a. The plane is horizontal and intersects the borehole centre. As shown in Fig. 6, after initiating along the perforation orientation, the HF in each case experienced a reorientation process until it finally propagated perpendicularly to the σ_3 orientation. The subfigures of Fig. 6 show the HF reorientation trajectories with different perforation angles.

4.1.2 RFPA3D Results and Their Comparison with XFEM Results

In RFPA, material heterogeneity is considered and simulated based on the Weibull distribution (Weibull 1951) as presented in Eq. (1)

$$f(u) = \frac{m}{u_0}\left(\frac{u}{u_0}\right)^{m-1}\exp\left(-\frac{u}{u_0}\right)^{m} \quad (1)$$

where $f(u)$ is the probability density function for a given u value, m is the homogeneity index (the higher the value of m, the more homogeneous the material), and u_0 is the mean value of the material property (i.e. Young's modulus or rock strength in this study).

To quantify the effect of rock heterogeneity on the overall rock mechanical properties, Liu et al. (2004) proposed two empirical formula (Eqs. 2, 3) to calculate the overall rock UCS and the rock Young's modulus based on the m values and the u_0 values. The relationship between different m values and rock overall properties is provided in Table 8.

$$\frac{\mathrm{UCS}}{\mathrm{UCS}_0} = 0.85928 - 0.80668\exp\left(-\frac{m}{10.68877}\right) \quad (2)$$

$$\frac{E}{E_0} = 1.02453 - 0.62081\exp\left(-\frac{m}{2.59074}\right) \quad (3)$$

Liu et al. (2004) noted that the m value for a typical rock material is about 2. To compare the RFPA results with the HF reorientation trajectories in Abass et al.'s experiment, the m value in each modelling case was assumed to be 5 to represent the rock sample in the laboratory, which is more homogeneous than the rock in the field.

The experimental environment in Abass et al.'s study was reproduced in (He et al. 2016c) and the simulated HF reorientation trajectories from orientated perforations are provided in Fig. 7. Figure 7a shows the model geometry and the section plane used to present the results. As shown in Fig. 7b–e, RFPA3D is capable of simulating the HF reorientation process from oriented perforations. The HF in each modelling case initiated along the perforation orientation and reorientated its path towards its preferred propagation direction, which is perpendicular to the σ_3 orientation.

Table 7 Sample properties in Abass et al.'s experiment (Abass et al. 1994)

Young's modulus	Poisson's ratio	Uniaxial compressive strength	Tensile strength
14.3 GPa	0.21	55.4 MPa	5.6 MPa
Density	Hydraulic conductivity	Biot's coefficient	Porosity
1710 kg/m^3	3.9 e^{-7}m/s	0.7	26.5%

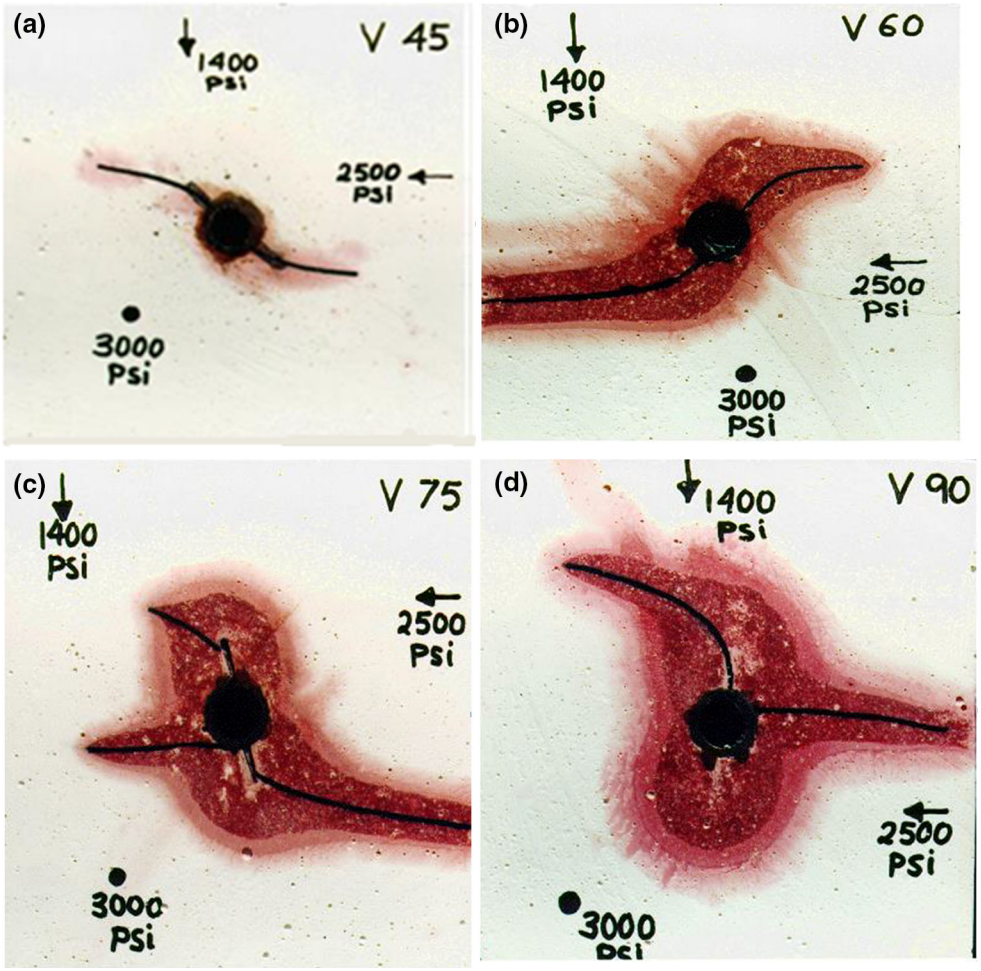

Fig. 6 HF reorientation trajectories with different perforation angles (Abass et al. 1994) (the section plane used to present the HF trajectory is illustrated in Fig. 7a): **a** the HF reorientation trajectory with a perforation angle of 45°; **b** the HF reorientation trajectory with a perforation angle of 60°; **c** the HF reorientation trajectory with a perforation angle of 75°; the HF reorientation trajectory with a perforation angle of 90°

Sepehri et al. (2015) used the eXtended finite element method (XFEM) to investigate the influencing factors in the HF reorientation process from orientated perforations. XFEM was developed in 1999 (Dolbow and Belytschko 1999). This method extends the traditional finite element method and introduces fracture mechanics to simulate crack problems without remeshing. Sepehri et al. (2015) validated XFEM's ability to simulate HF reorientation by reproducing the results in Abass et al.'s experiment with XFEM, which provides the possibility of examining the relative efficiency of RFPA3D and XFEM in simulating HF reorientation.

The simulation results of both RFPA3D and XFEM were superimposed on the laboratory results in Abass et al.'s study as shown in Fig. 8. The superimposed HF trajectories in each case indicate that RFPA3D exhibits a good ability to predict the HF reorientation trajectories when the perforation angles change from 45° to 75° as shown in Fig. 8b–d, respectively. In the extreme case where the perforation angle is 90° as shown in Fig. 8e, the RFPA result shows a little deviation from the laboratory result. Despite this, He et al. (2016c) found that the deviation only happened in the near-borehole area and the simulated HF gradually became aligned with the laboratory result when it propagated towards the model boundary (not shown in Fig. 8e). On the contrary, the XFEM result in each case exhibits a certain deviation from the laboratory result. As shown in Fig. 8, XFEM tends to overestimate the HF reorientation distance, which means the HF simulated by XFEM reorientates its path more slowly than the realistic result.

4.2 Hydraulic Fracture Reorientation Induced by the Stress Shadow Effect

4.2.1 Bunger et al.'s Laboratory Experiment

Bunger et al. (2011) carried out an experimental study on the interaction between closely located fractures in the cave

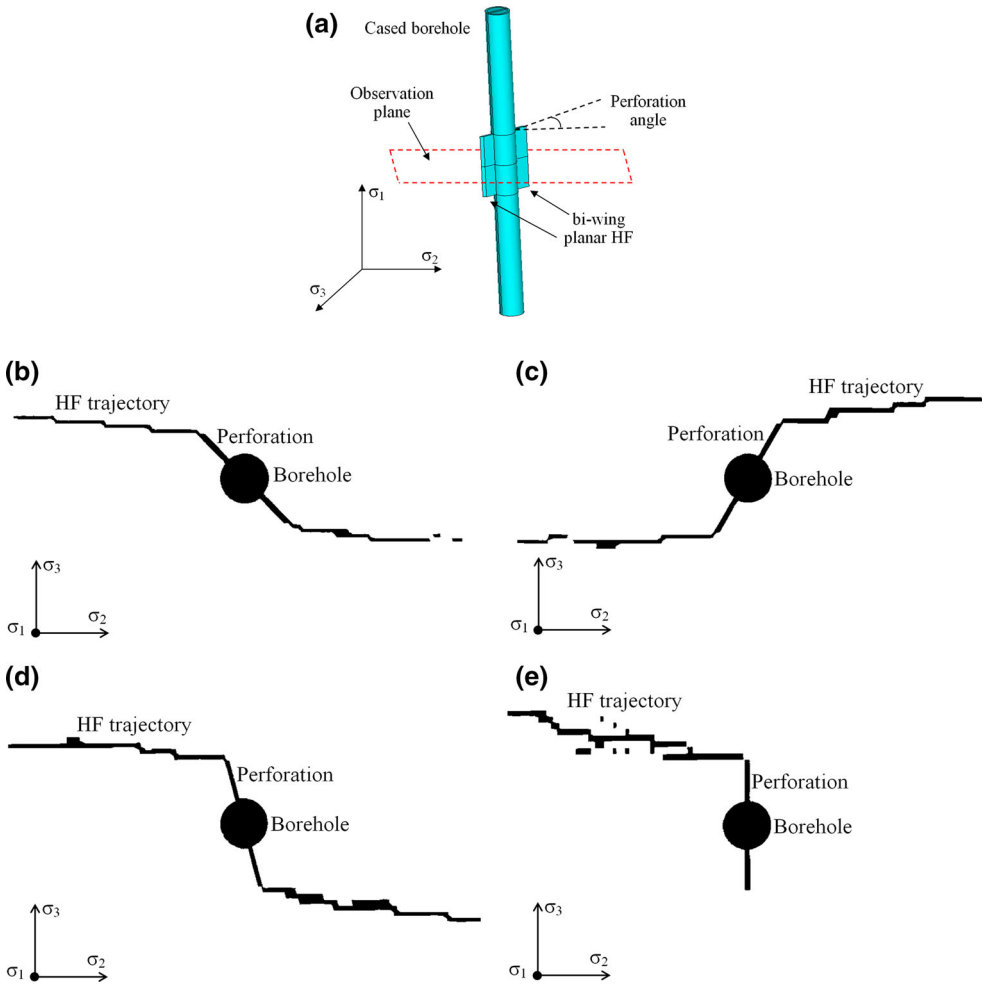

Fig. 7 Validation of RFPA's ability to simulate HF reorientation from orientated perforations: **a** the model geometry and the two-dimensional plane used to present the HF trajectory (the section plane is horizontal and intersects the borehole centre); **b** the RFPA result of HF reorientation with a perforation angle of 45°; **c** the RFPA result of HF reorientation with a perforation angle of 60°; **d** the RFPA result of HF reorientation with a perforation angle of 75°; **e** the RFPA result of HF reorientation with a perforation angle of 90°

Table 8 Relation between the overall rock property and its mean value with different *m* values

M	UCS_0 (MPa)	UCS (MPa)	UCS/UCS_0	E_0 (GPa)	*E* (GPa)	E/E_0
5	219	76.7	0.35	102 GPa	94.9 GPa	0.93
10	219	118.9	0.54	102	103.1	1.01
15	219	144.8	0.66	102	104.3	1.02

mining environment. A newly created HF that propagates too close to an existing fracture having a certain residual width may reorientate towards the latter one due to the induced stress shadow effect around the existing fracture. The experimental environment was designed based on the geotechnical condition at Cadia East Mine. Dimensional analysis (Barenblatt 1996) was applied to scale the model geometry and the input parameters. The HF trajectories in this study were well recorded and are selected as benchmarks for validating RFPA3D's ability to simulate HF reorientation induced by the stress shadow effect.

The HF in Bunger et al.'s experiment was the transverse radial HF, which is common in cave mining hydraulic fracturing. This HF type is different from that in Abass et al.'s experiment where the HF was the axial planar HF, which is common in the oil industry hydraulic fracturing. The rock samples used were blocks of Adelaide Black Granite with dimensions of 350 mm × 350 mm × 350 mm. A 16-mm-diameter vertical open borehole was drilled through the sample centre, and a diamond-coated steel tooth was used to cut 4 initial notches (1 mm in depth) around the borehole wall in the injection area. The notch orientation was aligned with the HF preferred propagation direction, and the notch was used to lower down the required breakdown pressure and ensure HF transverse initiation. The fracturing fluid had the viscosity of 0.58 Pa•s and was injected at a flow rate of 3^{-9} m^3/s. The sample properties are provided in Table 9.

The experiment results of Block 4 and Block 6 in Bunger et al.'s experiment were used to validate the

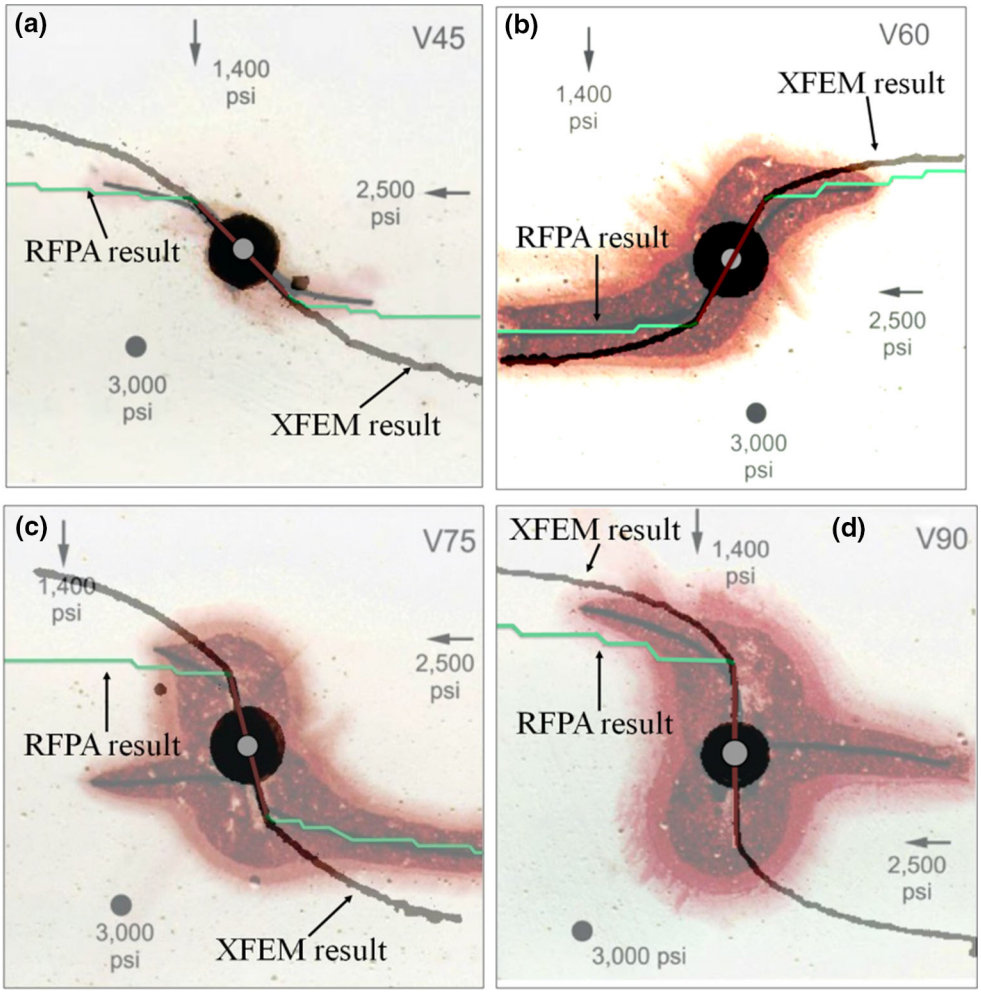

Fig. 8 Superimposition of HF trajectories simulated by RFPA and XFEM (Sepehri 2014) on HF trajectories observed in Bunger et al. (2011)'s experiment as provided in Fig. 6: **a** superimposed HF trajectories with a perforation angle of 45°; **b** superimposed HF trajectories with a perforation angle of 60°; **c** superimposed HF trajectories with a perforation angle of 75°; **d** superimposed HF trajectories with a perforation angle of 90°

simulation results. The stress states and the fracture spacings in these two cases are provided in Table 10. Figure 9 presents the section views of the HF trajectories in Block 4 and Block 6. The two-dimensional section plane used to present the HF trajectory is parallel to the σ_2–σ_3 plane and intersects the borehole as illustrated in Fig. 10a. In each case, the HFs were created in the order of 1 - 2 - 3 - 4. As shown in Fig. 9a, Fracture 2 (Fracture 4) reorientated its path and propagated towards Fracture 1 (Fracture 3) due to the stress shadow effect. In Fig. 9b, the HFs in Block 6, except Fracture 3, propagated parallel to each other, which means the stress shadow effect in this condition is not strong enough to induce HF reorientation. Bunger et al. (2011) thought the peculiar behaviour of Fracture 3 in Block 6 was due to the poor notch quality (Notch 3), and with this exception the condition in Block 6 favoured HFs parallel propagation.

4.2.2 RFPA3D Validation Results

The experimental environments in Block 4 and Block 6 were reproduced in (He et al. 2016b), and RFPA's ability

Table 9 Rock properties and the fluid viscosity in Bunger et al.'s experiment (Bunger et al. 2011)

Young's modulus	UCS	Tensile strength	Poisson's ratio
102 GPa	219 MPa	15 MPa	0.27
Density	Hydraulic conductivity	Biot's coefficient	Fluid viscosity
2970 kg/m^3	1 e^{-11} m/s	0.4	0.58 Pa s

Table 10 Stress states and fracture spacings in Block 4 and Block 6 (Bunger et al. 2011)

	σ_3 (MPa)	σ_{hmin} (MPa)	σ_{hmax} (MPa)	Fracture distance (mm)	Result
Block 4	0	4.6	4.6	15	Coalescence
Block 6	14.4	18	18	25	Sub-parallel

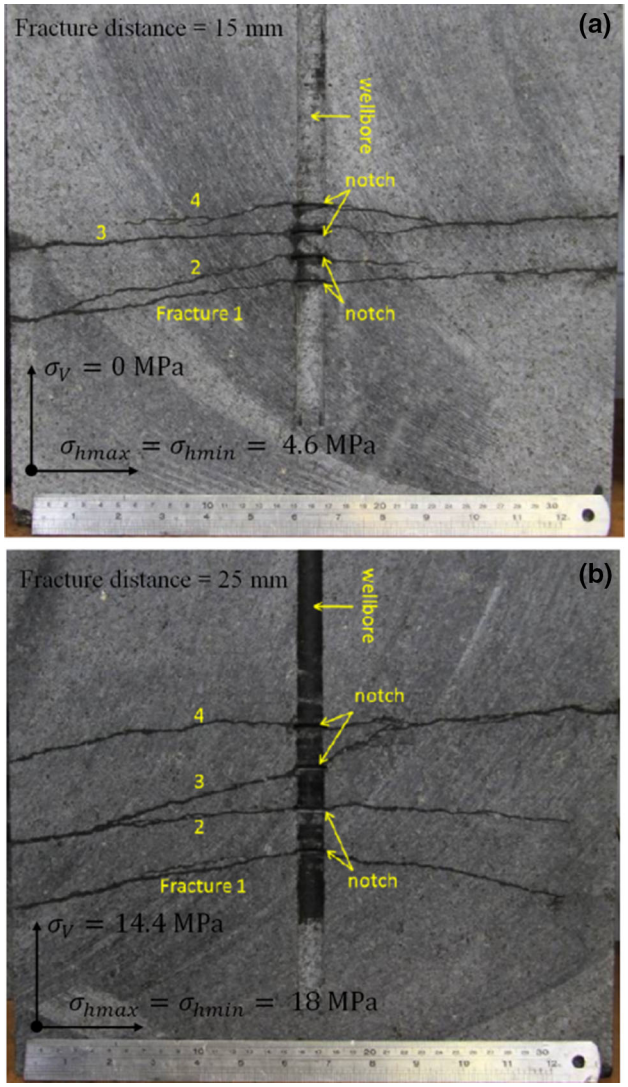

Fig. 9 HF trajectories recorded in Bunger et al. (2011)'s experiment (the section plane used to present the HF trajectory is illustrated in Fig. 10a): **a** the HF trajectories in Block 4 where the stress shadow effect is strong enough to induce HF reorientation; **b** the HF trajectories in Block 6 where the HFs propagate parallel to each other (except Fracture 3)

to simulate HF reorientation induced by the stress shadow effect was validated by comparing with the laboratory results.

To represent a pre-located fracture or a fracture with a certain residual width in numerical modelling, uniform tensile stress is applied to the fracture surfaces in previous studies (Olson 2008; Roussel and Sharma 2011a, b; Bunger et al. 2012; Manchanda and Sharma 2012; Roussel et al. 2012). The applied net pressure (i.e. the difference between the applied tensile stress and the closure stress) magnitude is equal to the needed stress that keeps the fracture having a certain propped width. For a plane strain fracture, which is common in the oil and gas industries, the net pressure magnitude can be calculated by Eq. (4) (Sneddon 1946)

$$\sigma_n = \frac{wE}{4(1-v^2)L_h} \tag{4}$$

For a radial fracture, which is common in the mining industry, the net pressure magnitude can be calculated by Eq. (5) (Tada et al. 2000)

$$\sigma_n = \frac{w\pi E}{8(1-v^2)r} \tag{5}$$

where r is the fracture radius.

In Bunger et al.'s experiment, the HF residual width was estimated to be about 0.01 mm (Bunger et al. 2011). In the numerical model, a net pressure of 2.5 MPa was applied on the fracture surfaces according to Eq. (5) to represent the existing HF. The model geometry is shown in Fig. 10a. The observation plane was consistent with that in Bunger et al.'s experiment and is provided in Fig. 10a. Three modelling cases were designed to validate the model's ability. In Case 1, the stress state in Block 4 was reproduced, but no pre-located fracture was simulated. This is to validate the model's ability to simulate a single HF propagation without the disturbance of the stress shadow effect. In Case 2 and Case 3, the conditions (i.e. the stress states and the fracture spacings) in Block 4 and Block 6 were reproduced, respectively. This is to validate the model's ability to reproduce the laboratory results in Bunger et al.'s study. Figure 10b–d presents the modelling results of Cases 1–3, respectively. These results indicate RFPA3D is capable of simulating a single HF propagation that is perpendicular to the in situ $\sigma 3$ orientation as shown in Fig. 10b. RFPA3D successfully reproduces the laboratory results in Bunger et al.'s study. In Fig. 10c, the newly created HF reorientates its path after initiating horizontally and propagates gradually towards the existing fracture, which is consistent with the laboratory result of Block 4 as shown in Fig. 9a. In Fig. 10d, the newly created HF propagates horizontally and is parallel to the existing fracture, which is consistent with the laboratory result of Block 6 as shown in Fig. 9b.

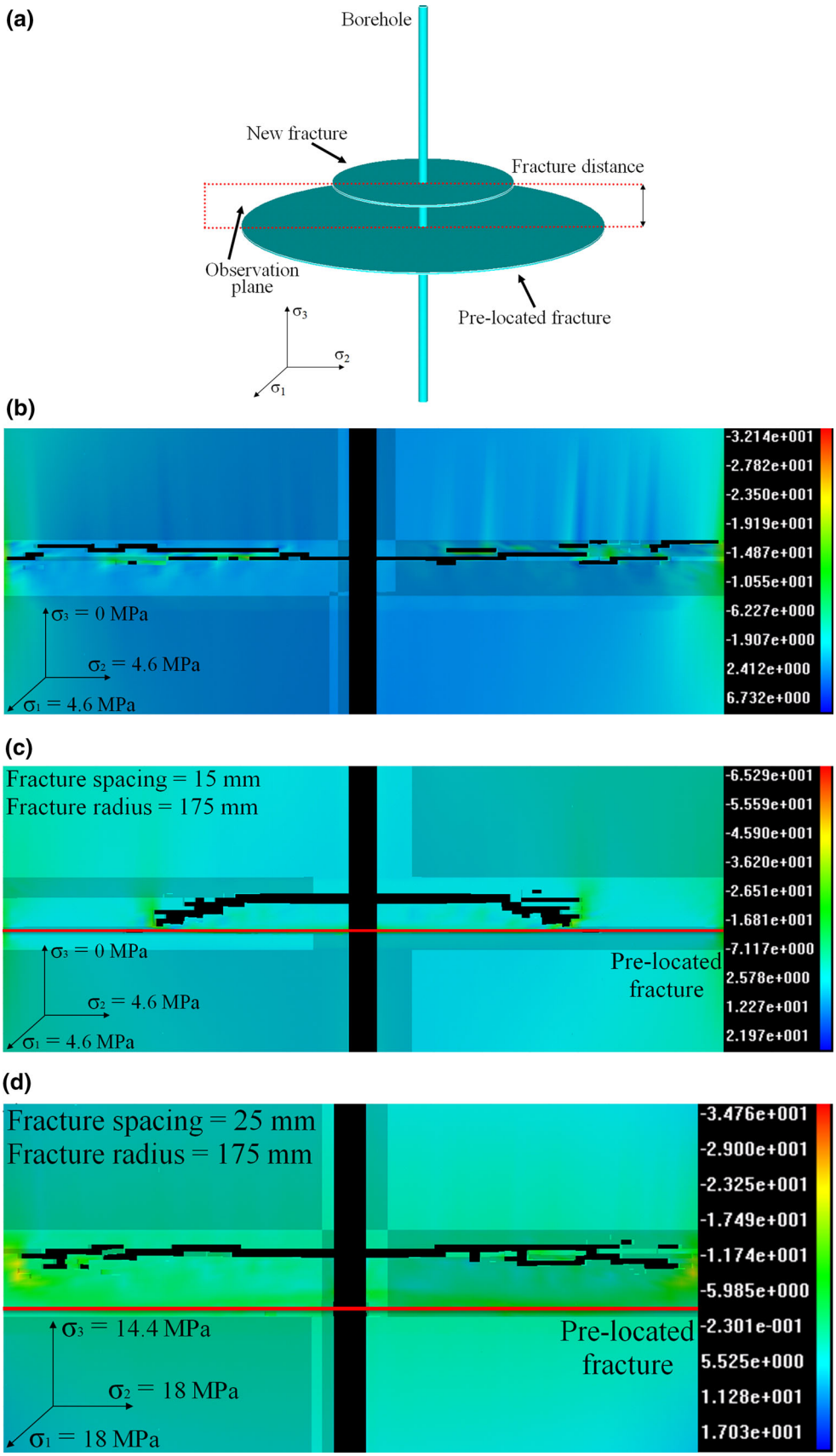

Fig. 10 Validation of RFPA's ability to simulate HF reorientation induced by the stress shadow effect: **a** the model geometry and the section plane used to present the HF trajectory (the section plane is parallel to the $\sigma_2 - \sigma_3$ plane and intersects the borehole centre); **b** the simulation of single HF propagation without the stress disturbance of a closely located fracture; **c** reproduction of the experiment result in Fig. 9a where HF reorientation occurs due to the stress shadow effect; **d** reproduction of the experiment result in Fig. 9b where the stress shadow effect is not strong enough to induce HF reorientation

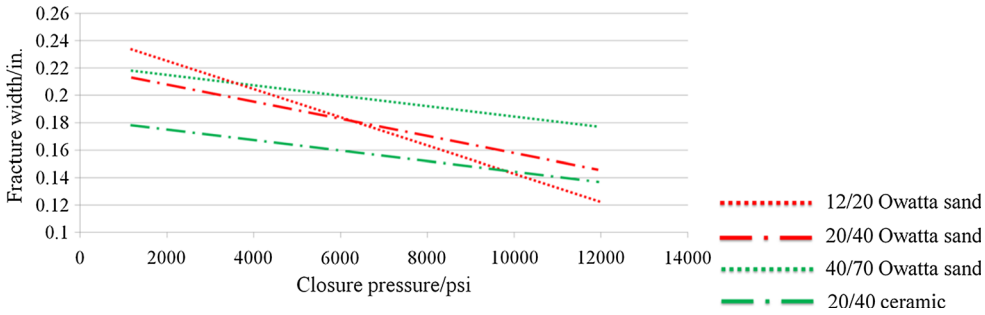

Fig. 11 Relation between the propped fracture width and the closure pressure when different types of proppants are used (Smith and Montgomery 2015)

5 Modelling Study on the Feasibility of Prescribed Hydraulic Fracturing

In this section, the validated modelling code, RFPA3D, is used to study the feasibility of prescribed hydraulic fracturing and its sensitivity to the in situ stress condition and rock properties. The numerical model is built in a laboratory-scale and reproduces the environment in Bunger et al.'s study (Bunger et al. 2011) to represent the geotechnical condition in cave mining.

5.1 Model Setup

5.1.1 Proppants and Their Effect on the Fracture Residual Width

In the oil and gas industries, proppants are normally used during or after hydraulic fracturing. This is to keep the HF having a certain residual width so that reservoir permeability is enhanced. In the mining industry, proppants have not been utilized for the purpose of preconditioning. The reason is that mining industry HFs function as artificial weakness planes that make the rock mass blocky. The HF is not required to be kept open as long as it is added into the rock mass. To realize the proposed approaches in Figs. 3b and 4b, the utilization of proppants is essential to change the local stress state between the pre-located fractures. Thus, proppants may also have potential applications in the mining industry. At this stage, sand is suggested for its low cost and satisfactory efficiency.

Smith and Montgomery (2015) provide the relationship between the pre-located fracture width and the closure stress when different types of sand are used as proppants. The results in Fig. 1 indicate the propped fracture width decreases linearly with the increase in the closure stress. For an orientation-uncontrollable HF, whose orientation is perpendicular to the far-field σ_3 orientation, the closure stress is equivalent to σ_3. The σ_3 magnitudes at Northparkes Mine and Cadia East Mine are 18 MPa (about 2500 psi) and 42 MPa (about 6000 psi), respectively (Jeffrey et al. 2009; Catalan et al. 2012). From Fig. 1, it shows in a low closure stress condition (Northparkes Mine) the propped fracture width may decrease by 5% compared with its maximum width, and the fracture may have a final width of 4.8–5.6 mm. In a high closure stress condition (Cadia East Mine), the propped fracture width may decrease by about 10% compared with its maximum width, and the fracture may have a final width of 4.5–5.3 mm (Fig. 11).

5.1.2 Model Assumptions

The schematic of the model is illustrated in Fig. 12a, and the overall model geometry is provided in Fig. 12b. Figure 12c describes the components of the model and the HF trajectory observation plane, which is parallel to the $\sigma_2-\sigma_3$ plane and passes through the borehole centre.

The numerical model is based on the following assumptions. The borehole lies on the σ_2–σ_3 plane and has a dip angle of 60°. This borehole dip angle is in a reasonable range because an acute dip angle (i.e. a sub-parallel borehole) increases the required number of boreholes to precondition a given rock mass and a sharp dip angle (i.e. a sub-vertical borehole) restricts HF reorientation induced by DHF. The pre-located fracture has a radius of 150 mm, and the fracture spacing is 100 mm. The L_d/r ratio is 2/3 and is much lower than that in Tables 1 and 2.

In the oil and gas industry, more viscous fracturing fluid (that result in wider fracture initial widths) and proppants are used. To avoid the strong stress shadow effect induced by pre-located fractures, the L_d/r ratio is normally higher than unity as listed in Tables 1 and 2. In the cave mining industry, water is normally used as fracturing fluid. This implies the pre-located fracture will have a narrower initial width. To take advantage of the stress shadow effect induced by pre-located fractures, a lower L_d/r ratio is required. In addition, a lower L_d/r ratio can lead to smaller fragmentation sizes that are favourable for cave propagation.

The in situ stress condition in each modelling case is assumed to be reverse faulting (i.e. in situ σ_3 is vertical), which is common at caving mine sites in Australia. The effect of σ_3, as the effect of the closure pressure, on the fracture width is assumed to be fixed to decrease the fracture width by 10%. The net pressure magnitude in each modelling case is assumed to be 2 MPa (has accounted for

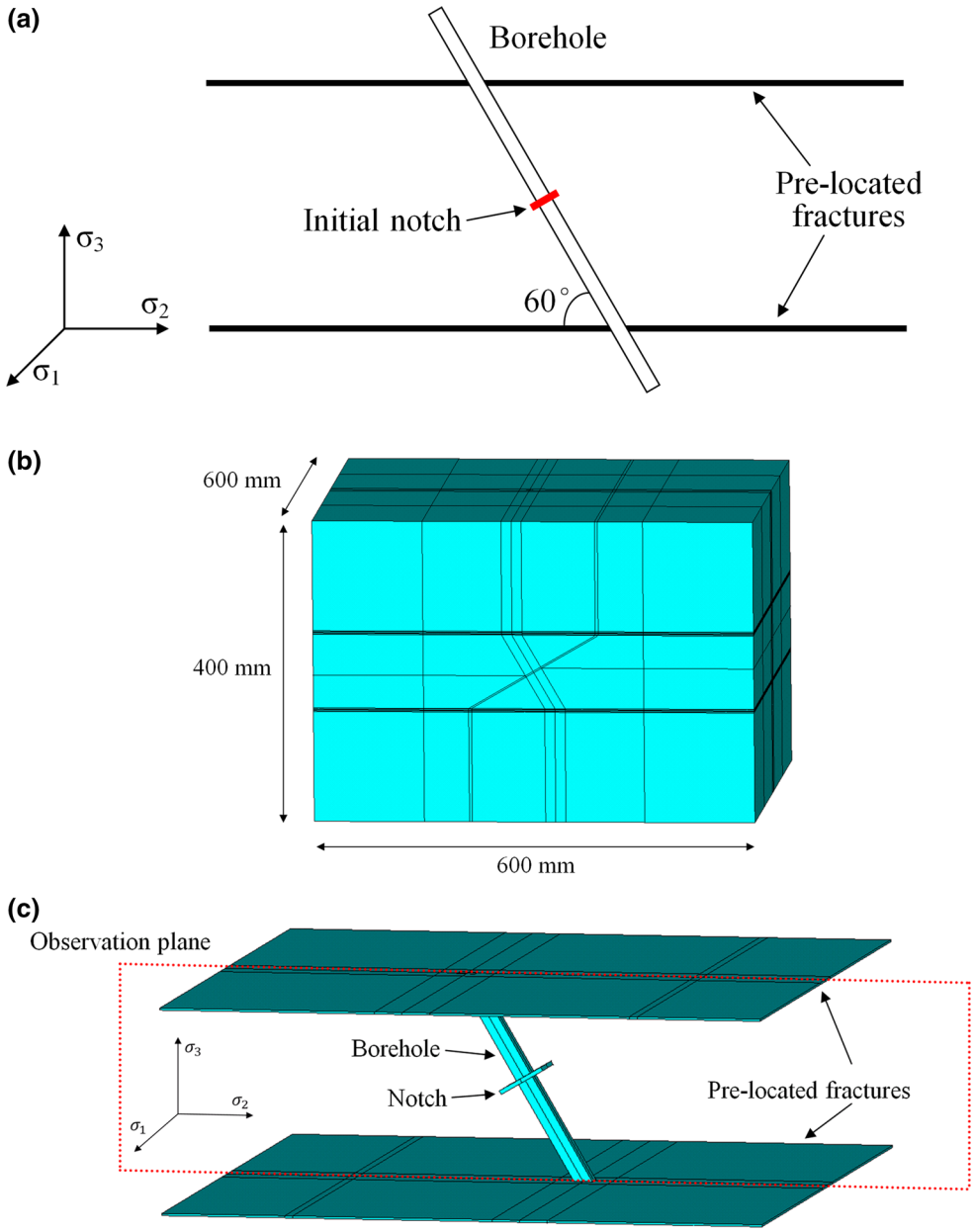

Fig. 12 Numerical model for simulating prescribed hydraulic fracturing: **a** the schematic of the model that shows an inclined borehole intersects the pre-located fractures with a 60° dip angle; **b** the model overall rock mass block that contains the model components in **c**; **c** model components and the HF observation plane (the section plane I parallel to the $\sigma_2-\sigma_3$ plane and passes through the borehole)

the influence of the closure stress). This net pressure magnitude is in a reasonable range. In Bunger et al.'s experiment, the pre-located fracture width was estimated to be about 0.01 mm, which results in a net pressure of about 2.5 MPa according to Eq. (5). Mills et al. (2004) performed stress change monitoring at Northparkes Mines. The induced stress change observed from monitoring instruments located 14–48 m above a single HF was from 0.5 to 1.4 MPa. An initial notch is created around the borehole wall at the middle of the pre-located fractures for the HF to initiate as shown in Fig. 12a, c.

5.2 Modelling Scenarios

The modelling scenarios are divided into 4 sets and are provided in detail in Tables 11 and 12. The basic input parameters are consistent with that in Bunger et al.'s experiment (Bunger et al. 2011) and is shown in Table 13. In each modelling scenario in Sets 1–3, the m value is assumed to be 5 to simulate a heterogeneous rock mass.

In Set 1, the feasibility of prescribed hydraulic fracturing and the role of in situ σ_3 in this process are examined. Earlier studies on the analytical solution to a HF with a

Table 11 Modelling scenarios to study the influence of the in situ stress condition on prescribed hydraulic fracturing

	σ_1 (MPa)	σ_2 (MPa)	σ_3 (MPa)
Set 1			
Case 1-1	31	16	10
Case 1-2	30	15	10
Case 1-3	20	13	10
Case 1-4	21	6	0
Case 1-5	20	5	0
Case 1-6	10	3	0
Set 2			
Case 2-1	1	1	0
Case 2-2	1.5	1.5	0
Case 2-3	2	2	0
Case 2-4	2.5	2.5	0
Set 3			
Case 3-1	5	5	0
Case 3-2	6	6	0
Case 3-3	7	7	0
Case 3-4	8	8	0

Table 12 Modelling scenarios to study the influence of rock mass properties on prescribed hydraulic fracturing

	UCS (MPa)	*m*
Set 4		
Case 4-1	175	5
Case 4-2	110	5
Case 4-3	219	10
Case 4-4	219	20

regular geometry show that the differential stress condition has no influence on the HF width and the HF length/radius for a given injection time (Khristianovic and Zheltov 1955; Perkins and Kern 1961; Geertsma and De Klerk 1969; Nordgren 1972; Geertsma and Haafkens 1979). The only influence of the in situ stress condition is on fluid pressure that is the sum of the net pressure and σ_3.

For a reoriented HF with an irregular geometry, previous studies found that the influencing factor related to the stress state on the HF trajectory is the differential stress rather than the absolute magnitude of each in situ principal stress component (Behrmann and Elbel 1991; Abass et al. 1994; Roussel and Sharma 2011a; Rafiee et al. 2012). The only effect of σ_3 on HF reorientation is decreasing the pre-located fracture width, which determines the extent of the stress shadow (Smith and Montgomery 2015).

In this paper, the problem being investigated is the prescribed hydraulic fracturing process. The dependent variable is the HF final propagation trajectory. The HF may propagate vertically as created by Approach One (Fig. 3b), inclinedly as created by Approach Two (Fig. 4b), or horizontally as dictated by the theoretical prediction. The HF trajectory is determined by many independent variables that include the in situ stress condition, rock properties, and the fracture spacing.

In Cases 1-1 to 1-3, realistic stress states (where $\sigma_3 \neq 0$ and $\sigma_1 > \sigma_2 > \sigma_3$) are simulated. In each case in Scenarios 1-1 to 1-3, the σ_3 magnitude is assumed to be 10 MPa to simulate the overburden stress. In Case 1-1, the differential stress state is close to that in the E48 orebody at Northparkes Mine (Jeffrey et al. 2009). In Case 1-2, the differential stresses are decreased slightly to create a low differential stress state that may favour the utilization of Approach Two (Fig. 4b) to create oblique PHFs. In Case 1-3, the differential stress state is close to that in the E26 orebody at Northparkes Mine (Van As and Jeffrey 2000a). The differential stress magnitudes in Case 1-3 are much lower than that in Cases 1-1 to 1-2 and may favour the utilization of Approach One (Fig. 3b) to create vertical PHFs. In each case in Cases 1-4 to 1-6, the σ_3 magnitude is assumed to be zero and the differential stress magnitudes are the same as that in Cases 1-1 to 1-3, respectively.

In Sets 2–3, the sensitivity of prescribed hydraulic fracturing to the in situ differential stress σ_d is studied. The stress conditions are based on that of Block 4 in Bunger et al.'s experiment (Bunger et al. 2011) where the stress magnitudes are $\sigma_3 = 0$ MPa and $\sigma_1 = \sigma_2 = 4.6$ MPa. The σ_3 magnitude in each modelling case in Sets 2 to 3 is assumed to be zero, and the σ_1 magnitude is equal to that of σ_2. In Set 2, the σ_d magnitude is increased from 1 MPa to 2.5 MPa, and the σ_n/σ_d ratio is decreased from 2.00 to 0.80. This is to keep the σ_n/σ_d ratio high enough to study the feasibility of Approach One. In Set 2, the σ_d magnitude is increased from 5 MPa to 8 MPa, and the σ_n/σ_d ratio is decreased from 0.40 to 0.25. This is to keep the σ_n/σ_d ratio at a low level to study the feasibility of Approach Two.

In Set 4, the sensitivity of prescribed hydraulic fracturing to rock properties is investigated. In each modelling case in Set 4, the stress condition is the same as that of Case 3-1 where $\sigma_3 = 0$ MPa and $\sigma_1 = \sigma_2 = 5$ MPa. In each modelling case, the ratio of rock UCS to rock tensile strength is kept constant at 14.6, which is consistent with the ratio in Table 13. In Cases 4-1 to 4-2, rock UCS is 175 MPa and 110 MPa, respectively, and is decreased by 20% and 50%, respectively, compared with the original value (219 MPa) as listed in Table 13. In Cases 3 to 4, the homogeneity index *m* values are 10 and 20, respectively, to simulate more homogeneous rock masses compared with that in Case 3-1. The relation between rock mass properties and different *m* values can be found in Table 8.

Table 13 Input parameters for studying the feasibility of prescribed hydraulic fracturing

Young's modulus	UCS	Tensile strength	Poisson's ratio	Density
102 GPa	219 MPa	15 MPa	0.27	2970 kg/m^3
Homogeneity index	Hydraulic conductivity	Biot's coefficient	Porosity	Fluid viscosity
5	1 e^{-11} m/s	0.4	5%	0.58 Pa s

5.3 Modelling Results and Discussion

5.3.1 Feasibility of Prescribed Hydraulic Fracturing and the Role of the Minimum In situ Principal Stress

The modelling results of Set 1 are provided in Fig. 13. Figure 13a–f presents the simulated HF trajectories in Cases 1-1 to 1-6, respectively, and the equivalent HF trajectories are plotted and superimposed in Fig. 13g for comparison.

As shown in Fig. 13a, in a high differential stress state (Case 1-1), the pre-located fractures fail to induce their connection with the newly created HF to form either a vertical PHF (Fig. 3b) or an oblique PHF (Fig. 4b). The HF propagates horizontally and parallel to the pre-located fractures after a reorientation process induced by DHF. In Fig. 13b, with the decrease in the differential stress magnitudes (Case 1-2), the newly created HF experiences a secondary reorientation process induced by the pre-located fractures and both its upper and lower strands connect the pre-located fractures to form an oblique PHF. This confirms the basic idea illustrated in Fig. 4b and indicates Approach Two should be applicable to creating PHFs that are not oblique to the in situ σ_3 orientation. In Case 1-3, the differential stresses have lower magnitudes and may favour the stress shadows overlap each other. As shown in Fig. 13c, the HF tends to propagate along the notch direction within a certain distance and then reorientate vertically towards the pre-located fractures. This implies the local stress state between the pre-located fractures is altered from the in situ stress state and the local σ_3 orientation in this region becomes that of the far-field σ_2. The basic idea of Approach One (Fig. 3b) is successfully realized in Case 1-3, and the modelling result shows this approach should be applicable to creating vertical PHFs that are parallel to the far-field σ_3 orientation.

In each case in Cases 1-4 to 1-6, the σ_3 magnitude is assumed to be zero. Compared with Case 1-1, Case 1-4 has a different in situ stress state but the same differential stress magnitude. Similarly, the differential stresses in Case 1-5 and Case 1-6 are equal to that in Case 1-2 and Case 1-3, respectively. As shown in Fig. 13d, the HF in Case 1-4 fails to connect the pre-located fractures and its final propagation path is horizontal as dictated by the theoretical prediction. This result is the same as that in Case 1-1. In Fig. 13e, f, an oblique PHF and a vertical PHF are created, respectively. These results are consistent with that in Case 1-2 and Case 1-3, respectively, where realistic stress states are simulated. The superimposed HF trajectories in Fig. 13g show that the HF propagation paths in the modelling cases that have the same differential stress magnitudes are very similar to each other. These results indicate the change in the σ_3 magnitude in two modelling cases that have the same differential stress magnitudes does not influence the HF reorientation process as long as other independent variables are kept constant. For example, Case 1-2 and Case 1-4 have the same differential stresses but differential in situ principal stress magnitudes. In Case 1-2 where a realistic stress state is simulated, an oblique PHF is created as shown in Fig. 13b. In Case 1-4, the σ_3 magnitude is decreased from 10 MPa to 0 MPa. As shown in Fig. 13d, g, compared with the HF trajectory in Case 1-2, the change in the σ_3 magnitude in Case 1-4 does not either further reorientates the HF to form a vertical PHF as depicted in Fig. 3a or restricts HF reorientation so that the HF fails to connect the pre-located fractures. In addition, the HF trajectories in both cases are similar to each other.

As discussed in Sect. 5.1.1, the increase in the σ_3 magnitude will decrease the propped fracture width, which restricts HF reorientation. However, as shown in Fig. 11, the reduction in the propped fracture width due to the closure stress is limited and may only reach 10% of the fracture maximum width in a high σ_3 stress state.

5.3.2 Sensitivity to the Differential Stress

The modelling results of Set 2 and Set 3 are provided in Figs. 14 and 15, respectively. Figure 14a–d presents the simulated HF trajectories in Cases 2-1 to 2-4, respectively. The equivalent HF trajectories in these cases are superimposed in Fig. 14e for comparison. Figure 15a–d presents the simulated HF trajectories in Cases 3-1 to 3-4, respectively. The equivalent HF trajectories in these cases are superimposed in Fig. 15e for comparison.

As shown in Fig. 14a–d, Approach One is successfully realized in Cases 2-1 to 2-4 where lower σ_d magnitudes are simulated. In each case, the HF initiates along the notch direction and then reorientates its path towards the pre-located fractures to form a vertical PHF. To realize Approach One where a stress reversal region occupies the whole space between the pre-located fractures, the net pressure magnitude does not need to be higher than that of

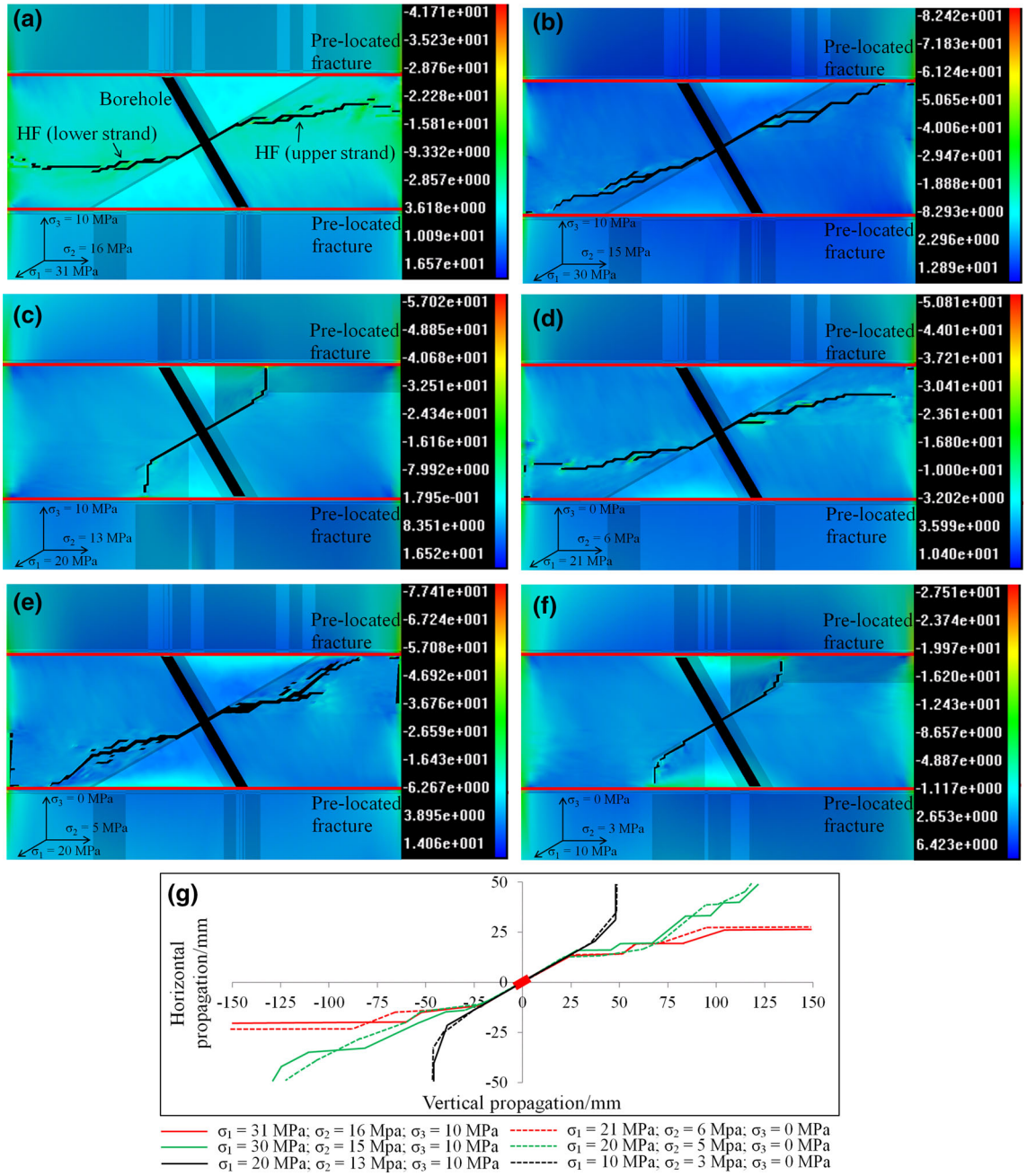

Fig. 13 Modelling results of Set 1 and superimposed HF trajectories (the legend and contour show the σ_3 distribution): **a** the HF trajectory in Case 1-1 where $\sigma_1 = 31$ MPa, $\sigma_2 = 16$ MPa, and $\sigma_3 = 10$ MPa; **b** the HF trajectory in Case 1-2 where $\sigma_1 = 30$ MPa, $\sigma_2 = 15$ MPa, and $\sigma_3 = 10$ MPa; **c** the HF trajectory in Case 1-3 where $\sigma_1 = 20$ MPa, $\sigma_2 = 13$ MPa, and $\sigma_3 = 10$ MPa; **d** the HF trajectory in Case 1-4 where $\sigma_1 = 21$ MPa, $\sigma_2 = 6$ MPa, and $\sigma_3 = 0$ MPa; **e** the HF trajectory in Case 1-5 where $\sigma_1 = 20$ MPa, $\sigma_2 = 5$ MPa, and $\sigma_3 = 0$ MPa; **f** the HF trajectory in Case 1-6 where $\sigma_1 = 10$ MPa, $\sigma_2 = 3$ MPa, and $\sigma_3 = 0$ MPa; **g** the superimposed HF trajectories in Set 1 that indicate HFs with the same differential stresses have similar trajectories

the in situ differential stress as long as the pre-located fracture spacing is close enough as proved in Cases 1-3 to 1-4. From the superimposed HF trajectories in Fig. 14e, the σ_n/σ_d ratio determines the HF reorientation distance in each modelling case. As shown in Fig. 14e, the HF reorientates more quickly towards the pre-located fractures with a higher σ_n/σ_d ratio. This implies pre-located fractures can effectively change the local stress state between them. A high σ_n/σ_d ratio increases the local differential stress and hence speeds up the HF reorientation process.

The simulation results in Set 3 indicate the feasibility of Approach Two is very sensitive to the σ_n/σ_d ratio. In Case 2-1 (Fig. 15a), Approach Two is realized to create an oblique PHF. The HF tends to propagate horizontally after

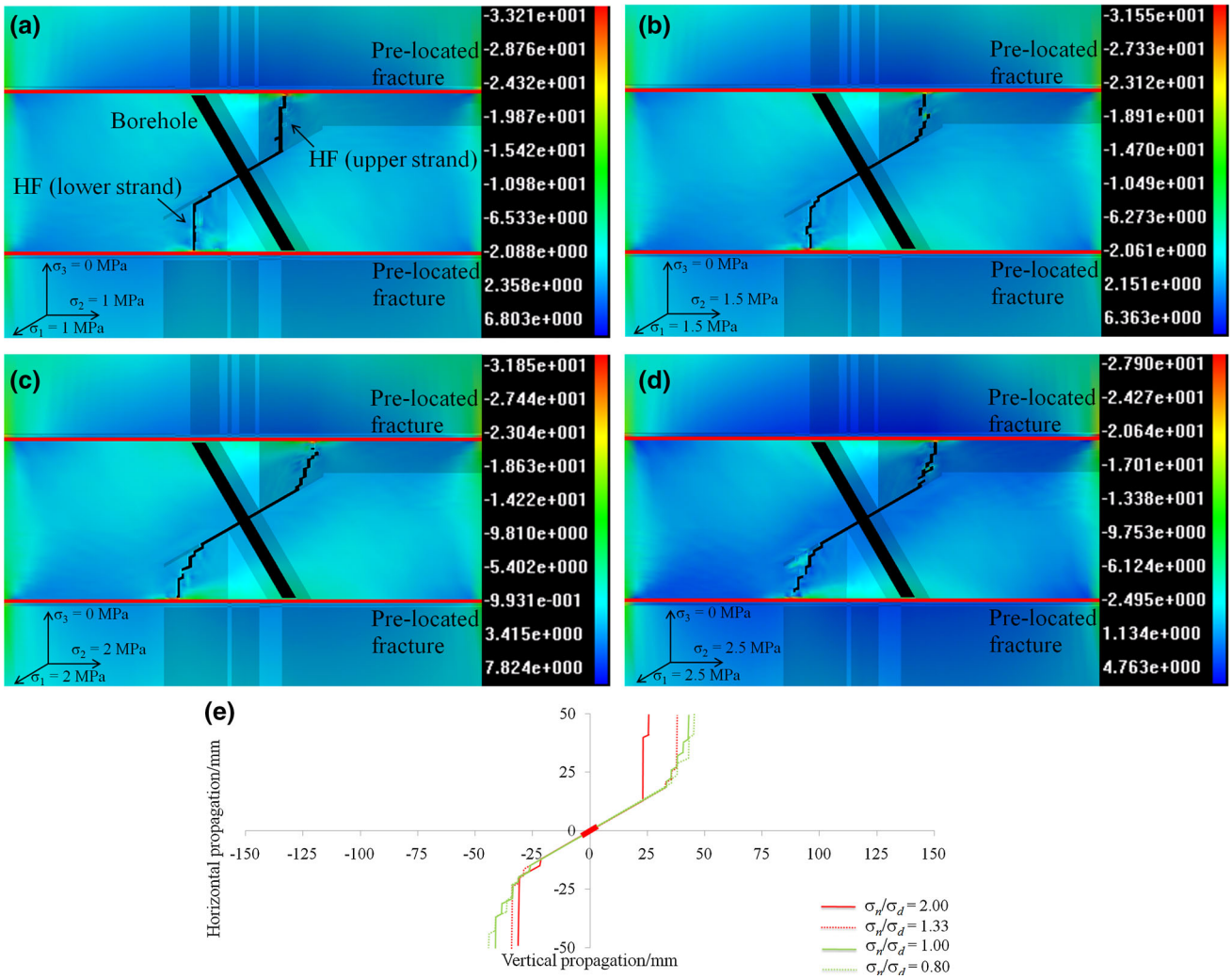

Fig. 14 Modelling results of Set 2 and superimposed HF trajectories (the legend and contour show the σ_3 distribution): **a** the HF trajectory in Case 2-1 where $\sigma_d = 1$ MPa, $\sigma_n = 2$ MP; **b** the HF trajectory in Case 2-2 where $\sigma_d = 1.5$ MPa, $\sigma_n = 2$ MP; **c** the HF trajectory in Case 2-3 where $\sigma_d = 2$ MPa, $\sigma_n = 2$ MP; **d** the HF trajectory in Case 2-4 where $\sigma_d = 2.5$ MPa, $\sigma_n = 2$ MP; **e** superimposed HF trajectories in Set 2 that show the change in the HF trajectory with different σ_n/σ_d ratios

initiating along the notch direction and then experiences a secondary reorientation process that induces the HF to propagate towards the pre-located fractures. The overall HF orientation is oblique and is not perpendicular to the far-field σ_3 orientation. The result in Case 3-1 also shows to realize Approach Two, the net pressure magnitude does not need to be higher than that of the in situ differential stress as the σ_n/σ_d ratio in Case 3-1 is 0.4. When the σ_n/σ_d ratio is decreased from 0.33 to 0.25 (Case 3-2, Case 3-3, and Case 3-4), the HF fails to connect the pre-located fractures and propagates horizontally after initiating obliquely along the notch direction. The results in both sets also indicate that HF reorientation from an artificial weakness is not necessarily a near-borehole effect that confines the HF reorientation distance within one or two borehole diameters. In a low differential stress state, the HF tends to propagate along the prescribed notch direction within a long distance.

As shown in Fig. 14, the HF reorientation distance in Approach One exceeds two borehole diameters and tends to be longer with a lower σ_n/σ_d ratio. On the contrary, the HF reorientation distance in Approach Two decreases with a lower σ_n/σ_d ratio as shown in Fig. 15. Although the local σ_3 orientation between the pre-located fractures in Approach Two is still aligned with the far-field σ_3 orientation, the pre-located fractures are proved to be efficient in decreasing the local differential stress magnitude and are favourable for the utilization of DHF to prescribe the HF trajectory.

5.3.3 *Sensitivity to Rock Properties*

The equivalent HF trajectories in Set 4 are plotted in Fig. 16. In Fig. 16a, the HF trajectories in Case 4-1, Case 4-2, and Case 3-1 are superimposed for comparison. These

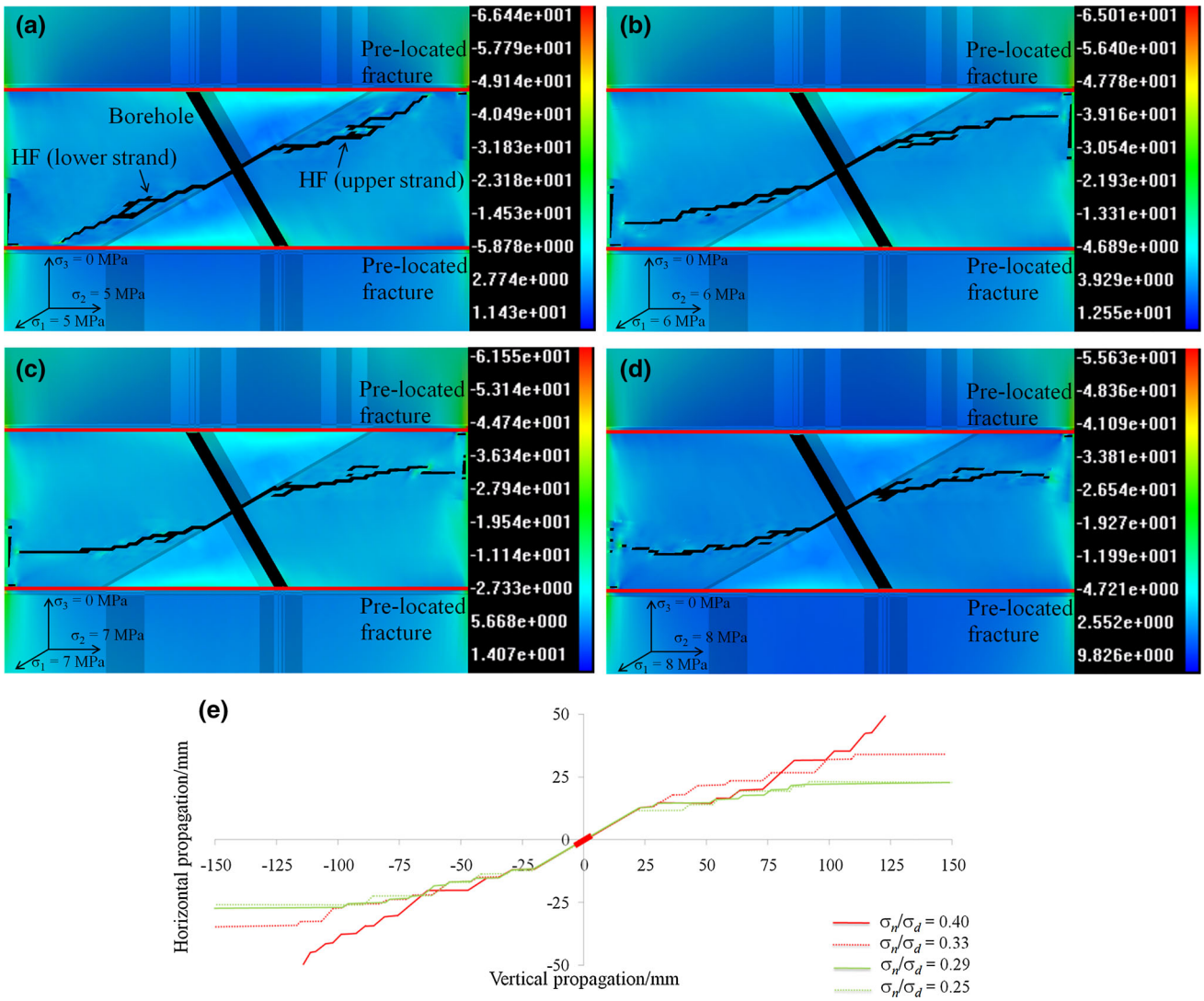

Fig. 15 Modelling results of Set 3 and superimposed HF trajectories (the legend and contour show the σ_3 distribution): **a** the HF trajectory in Case 3-1 where $\sigma_d = 5$ MPa, $\sigma_n = 2$ MP; **b** the HF trajectory in Case 3-2 where $\sigma_d = 6$ MPa, $\sigma_n = 2$ MP; **c** the HF trajectory in Case 3-3 where $\sigma_d = 7$ MPa, $\sigma_n = 2$ MP; **d** the HF trajectory in Case 3-4 where $\sigma_d = 8$ MPa, $\sigma_n = 2$ MP; **e** superimposed HF trajectories in Set 3 that show the change in the HF trajectory with different σ_n/σ_d ratios

cases have the same input parameters expect different rock strength (i.e. rock UCS and rock tensile strength). In Fig. 16b, the HF trajectories in Case 4-3, Case 4-4, and Case 3-1 are superimposed for comparison. These cases have the same input parameters expect different m values. The results in Fig. 16 indicate the PHF trajectory is sensitive to both rock strength and rock mass homogeneity.

In Fig. 16a, the HF tends to propagate horizontally in a weaker rock mass. The HF in Case 3-1 (UCS = 219 MPa) propagates inclinedly, and both its upper and lower strands connect the pre-located fracture to form an oblique PHF as depicted in Fig. 4b. The HF in Case 4-1 (UCS = 175 MPa) has its upper strand connecting the pre-located fracture with its lower strand propagating horizontally after the reorientation induced by DHF. The HF in Case 4-2 (UCS = 110 MPa) fails to connect either of the pre-located fractures and has the shortest reorientation distance compared with the other HFs. These results imply that rock strength also has important influence on HF reorientation. The influence of the differential stress, which restricts HF reorientation, could be more obvious in weaker rock masses.

The results in Fig. 16b indicate that rock mass homogeneity is another important factor that should be accounted for if the prediction of the HF reorientation trajectory is required. The HF in each modelling case in Fig. 16b succeeds in having its both strands connecting the pre-located fractures. However, the HF in Case 3-1 ($m = 5$) has the longest reorientation distance before it finally reaches the pre-located fractures. In more homogeneous rock masses

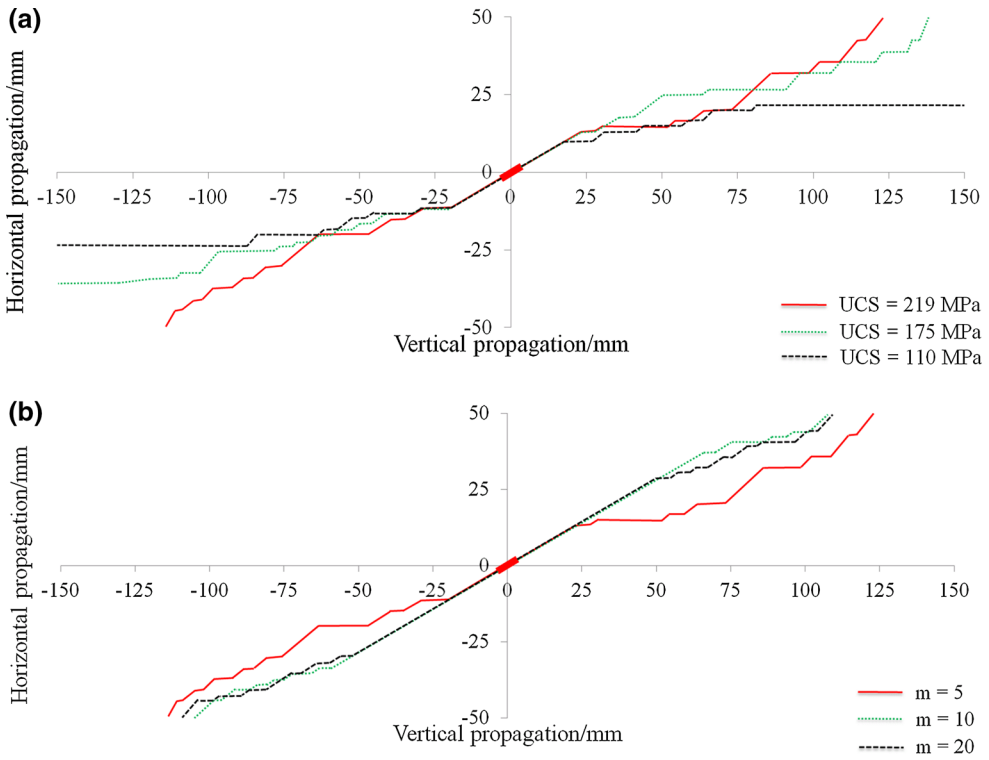

Fig. 16 Sensitivity of prescribed hydraulic fracturing to rock mass properties: **a** superimposed HF trajectories in Case 3-1 (UCS = 219 MPa), Case 4-1 (UCS = 175 MPa), and Case 4-2 (UCS = 110 MPa) that show the change in the HF trajectory with different rock UCS; **b** superimposed HF trajectories in Case 3-1 ($m = 5$), Case 4-3 ($m = 10$), and Case 4-4 ($m = 20$) that show the change in the HF trajectory with different homogeneity index m values

(i.e. Case 4-3 and Case 4-4 where the m values are 10 and 20, respectively), the HF tends to propagate more quickly towards the pre-located fractures with a shorter reorientation distances. These results imply that rock mass heterogeneity may not influence the feasibility of prescribed hydraulic fracturing but has certain influence on the HF trajectory. In addition, the similar HF trajectories in Case 4-3 ($m = 10$) and Case 4-4 ($m = 20$) show that the influence of the increment of rock mass heterogeneity on the HF trajectory might be negligible if m is above a critical value and the traditional material homogeneity assumption is valid to predict the HF path in this situation.

6 Conclusions

Hydraulic fracturing has been applied to cave mining to precondition the orebody with the purposes of improving rock mass caveability and reducing fragmentation sizes. He et al. (2016a) identified the limitation in current cave mining hydraulic fracturing applications and proposed the concept of prescribed hydraulic fracturing so that successful preconditioning can be realized in any geotechnical condition. In this paper, the feasibility of the proposed approaches to creating PHFs is discussed based on the review of previous studies on the stress shadow effect, DHF, and HF reorientation from oriented perforations. A validated numerical code, RFPA 3D is used to simulate PHFs created by both approaches in an experimental-scale model. The influence of the in situ stress condition and rock mass properties on prescribed hydraulic fracturing is investigated. The following conclusions are made.

Both approaches to creating PHFs are realized by numerical modelling and may be feasible in field applications. The HF orientation is not necessarily perpendicular to the far-field σ_3 orientation provided pre-located fractures are pre-located to modify the local stress state. Pre-located fractures can either create a stress reversal region that is required in Approach One, or decrease the local differential stress magnitude in the shadow-free zone occurred in Approach Two. Proppants, such as sand, are suggested to be utilized in future hydraulic fracturing operations in cave mining for the purpose of creating PHFs. The influencing factors related to the in situ stress state on prescribed hydraulic fracturing are differential stresses magnitudes (i.e. $\sigma_1-\sigma_3$ and $\sigma_2-\sigma_3$) rather than the absolute magnitudes of principal stresses. If other influencing factors are kept constant, prescribed hydraulic fracturing in two geotechnical conditions with different in situ stress states but the same differential stresses reaches the same result. The

feasibility of the proposed approaches is sensitive to the σ_n/σ_d ratio. The net pressure does not necessarily need to be higher than the in situ differential stress as long as the L_d/r ratio is sufficiently low. In a specific mine site, the σ_n/σ_d ratio is almost uncontrollable because the σ_n magnitude is related to the utilized fracturing fluid, which is normally water in cave mining, and the σ_d magnitude is determined by the in situ stress condition. At a mine site with a low σ_n/σ_d ratio, the proposed approach can be realized by decreasing the L_d/r ratio (i.e. by either decreasing the fracture spacing or increasing the fracture radius). Prescribed hydraulic fracturing is also sensitive to rock strength and rock mass heterogeneity. High rock strength may weaken the influence of the differential stress on HF reorientation and hence favours creating PHFs that are not perpendicular to the far-field σ_3 orientation. Rock mass heterogeneity may not influence the feasibility of prescribed hydraulic fracturing but has certain influence on the HF trajectory. In a more homogeneous rock mass, the HF tends to propagate more quickly towards the pre-located fractures with a shorter reorientation distance.

Acknowledgements The authors would like to thank Professor Chunan Tang and Mr. Jian Liu. Professor Chunan Tang is the founder and CTO of the RFPA code, and Mr. Jian Liu provided support in the use of RFPA 3D—Flow Version. The authors also thank Zecheng Li (PhD candidate) for his support.

References

Abass HH, Brumley JL, Venditto JJ (1994) Oriented perforations-a rock mechanics view. In: SPE annual technical conference and exhibition, Society of Petroleum Engineers

Abass HH, Hedayati S, Meadows D (1996) Nonplanar fracture propagation from a horizontal wellbore: experimental study. SPE Prod Facil 11(03):133–137

Adachi J, Siebrits E, Peirce A, Desroches J (2007) Computer simulation of hydraulic fractures. Int J Rock Mech Min Sci 44(5):739–757

Anderson TL, Anderson T (2005) Fracture mechanics: fundamentals and applications. CRC Press, Boca Raton

Barenblatt GI (1996) Scaling, self-similarity, and intermediate asymptotics: dimensional analysis and intermediate asymptotics. Cambridge University Press, Cambridge

Behrmann L, Elbel J (1991) Effect of perforations on fracture initiation. J Petrol Technol 43(05):608–615

Brzovic A, Rogers S, Webb G, Hurtado J, Marin N, Schachter P, Alvarez J, Baraona K (2015) Discrete fracture network modelling to quantify rock mass pre-conditioning at the El Teniente Mine, Chile. Min Technol 124(3):163–177

Bunger A, Jeffrey R, Kear J, Zhang X, Morgan M (2011) Experimental investigation of the interaction among closely spaced hydraulic fractures. In: 45th US rock mechanics/geomechanics symposium, American Rock Mechanics Association

Bunger AP, Zhang X, Jeffrey RG (2012) Parameters affecting the interaction among closely spaced hydraulic fractures. SPE J 17(01):292–306

Catalan A, Dunstan G, Morgan M, Green S, Jorquera M, Thornhill T, Onederra I, Chitombo G (2012) How can an intensive preconditioning concept be implemented at mass mining method? Application to Cadia East panel caving project. In: 46th US rock mechanics/geomechanics symposium, American Rock Mechanics Association

Chacon E, Barrera V, Jeffrey R, van As A (2004) Hydraulic fracturing used to precondition ore and reduce fragment size for block caving. In: Proceedings MassMin2004, pp 429–534

Chen M, Jiang H, Zhang G, Jin Y (2010) The experimental investigation of fracture propagation behavior and fracture geometry in hydraulic fracturing through oriented perforations. Pet Sci Technol 28(13):1297–1306

Cheng Y (2009) Boundary element analysis of the stress distribution around multiple fractures: implications for the spacing of perforation clusters of hydraulically fractured horizontal wells. In: SPE Eastern regional meeting, Society of Petroleum Engineers

Chernov O (1982) Hydrodynamic stratification of petrologically uniform strong rocks as a means of controlling intransigent roofs. J Min Sci 18(2):102–107

Chernov O, Kyu N (1996) Oriented rupture of solids by highly viscous fluid. J Min Sci 32(5):362–367

Chernov O, Barsukov I, Posokhov G (1997) Oriented hydraulic fracturing of a mass of rocks enclosing the "international" diamond pipe. J Min Sci 33(6):582–586

Chitombo G (2010) Cave mining: 16 years after Laubscher's 1994 paper'Cave mining–state of the art. Min Technol 119(3):132–141

Clark J (1949) A hydraulic process for increasing the productivity of wells. J Pet Technol 1(01):1–8

Daneshy AA (1971) True and apparent direction of hydraulic fractures. In: Drilling and rock mechanics conference, Society of Petroleum Engineers

Daneshy AA (1973a). Experimental investigation of hydraulic fracturing through perforations. J Pet Technol 25(10):1,201–201,206

Daneshy AA (1973b) A study of inclined hydraulic fractures. Soc Pet Eng J 13(02):61–68

Dolbow J, Belytschko T (1999) A finite element method for crack growth without remeshing. Int J Numer Meth Eng 46(1):131–150

Elbel JL, Mack MG (1993) Refracturing: observations and theories. In: Proceedings, SPE 25464, SPE production operations symposium, Society of Petroleum Engineers, Oklahoma City, Oklahoma, 21–23 March

Fan J, Dou L, He H, Du T, Zhang S, Gui B, Sun X (2012) Directional hydraulic fracturing to control hard-roof rockburst in coal mines. Int J Min Sci Technol 22(2):177–181

Geertsma J, De Klerk F (1969) A rapid method of predicting width and extent of hydraulically induced fractures. J Pet Technol 21(12):1,571–571,581

Geertsma J, Haafkens R (1979) A comparison of the theories for predicting width and extent of vertical hydraulically induced fractures. J Energy Res Technol 101(1):8–19

Geilikman M, Xu G, Wong S-W (2013) Interaction of multiple hydraulic fractures in horizontal wells. In: SPE unconventional gas conference and exhibition, Society of Petroleum Engineers

Guangqing Z, Mian C (2009) Complex fracture shapes in hydraulic fracturing with orientated perforations. Pet Explor Dev 36(1):103–107

He H, Dou L, Fan J, Du T, Sun X (2012) Deep-hole directional fracturing of thick hard roof for rockburst prevention. Tunn Undergr Space Technol 32:34–43

He Q, Suorineni F, Oh J (2015) Modeling interaction between natural fractures and hydraulic fractures in block cave mining. In: 49th US rock mechanics/geomechanics symposium, American Rock Mechanics Association

He Q, Suorineni F, Oh J (2016a) Review of hydraulic fracturing for pre-conditioning in cave mining. Rock Mech Rock Eng. doi:10.1007/s00603-016-1075-0

He Q, Suorineni FT, Ma T, Oh, J (2016b) Modelling directional hydraulic fractures in heterogeneous rock masses. In: Proceedings Seventh International Conference and Exhibition on Mass Mining (MassMin 2016), The Australasian Institute of Mining and Metallurgy, Melbourne, pp 369–384

He Q, Suorineni F, Oh J, Ma T (2016c) Modeling directional hydraulic fractures in heterogeneous rock masses. MassMin, Sydney

Huang B, Liu C, Fu J, Guan H (2011) Hydraulic fracturing after water pressure control blasting for increased fracturing. Int J Rock Mech Min Sci 48(6):976–983

Huang B, Wang Y, Cao S (2015) Cavability control by hydraulic fracturing for top coal caving in hard thick coal seams. Int J Rock Mech Min Sci 74:45–57

Hubbert MK, Willis DG (1972) Mechanics of hydraulic fracturing. Am Assoc Pet Geol 18:239–257

Jeffrey RG (2000) Hydraulic fracturing of ore bodies. Google Patents

Jeffrey R, Mills K (2000). Hydraulic fracturing applied to inducing longwall coal mine goaf falls. In: 4th North American rock mechanics symposium, American Rock Mechanics Association

Jeffrey R, Zhang X, Settari A, Mills K, Detournay E (2001) Hydraulic fracturing to induce caving: fracture model development and comparison to field data. In: DC Rocks 2001, The 38th US symposium on rock mechanics (USRMS), American Rock Mechanics Association

Jeffrey RG, Bunger A, Lecampion B, Zhang X, Chen Z, van As A, Allison DP, De Beer W, Dudley JW, Siebrits E (2009) Measuring hydraulic fracture growth in naturally fractured rock. In: SPE annual technical conference and exhibition, Society of Petroleum Engineers

Jeffrey R, Chen Z, Mills K, Pegg S (2013) Monitoring and measuring hydraulic fracturing growth during preconditioning of a roof rock over a coal longwall panel. In: ISRM international conference for effective and sustainable hydraulic fracturing, International Society for Rock Mechanics

Joubert P (2010) Microseismic monitoring of hydraulic fractures in block cave mines. Min Technol 119(3):193–197

Kaiser PK, Valley B, Dusseault MB, Duff D (2013) Hydraulic fracturing mine back trials—design rationale and project status. In: ISRM international conference for effective and sustainable hydraulic fracturing, International Society for Rock Mechanics

Katsaga T, Riahi A, DeGagne D, Valley B, Damjanac B (2015) Hydraulic fracturing operations in mining: conceptual approach and DFN modeling example. Min Technol 124(4):255–266

Kear J, White J, Bunger AP, Jeffrey R, Hessami M-A (2013) Three dimensional forms of closely-spaced hydraulic fractures. In: ISRM international conference for effective and sustainable hydraulic fracturing, International Society for Rock Mechanics

Khristianovic S, Zheltov Y (1955) Formation of vertical fractures by means of highly viscous fluids. In: Proceedings of 4th world petroleum congress, Rome

Laubscher D (1994) Cave mining-the state of the art. J S Afr Inst Min Metall 94(10):2279

Lekontsev YM, Sazhin P (2008) Application of the directional hydraulic fracturing at Berezovskaya Mine. J Min Sci 44(3):253–258

Lekontsev YM, Sazhin P (2014) Directional hydraulic fracturing in difficult caving roof control and coal degassing. J Min Sci 50(5):914–917

Li LC, Tang CA, Tham LG, Yang TH, Wang SH (2005) Simulation of multiple hydraulic fracturing in non-uniform pore pressure field. Adv Mater Res 9:163–172

Li L, Tang C, Li G, Wang S, Liang Z, Zhang Y (2012) Numerical simulation of 3D hydraulic fracturing based on an improved flow-stress-damage model and a parallel FEM technique. Rock Mech Rock Eng 45(5):801–818

Liu H, Roquete M, Kou S, Lindqvist P-A (2004) Characterization of rock heterogeneity and numerical verification. Eng Geol 72(1):89–119

Manchanda R, Sharma MM (2012). Impact of completion design on fracture complexity in horizontal wells. In: SPE annual technical conference and exhibition, Society of Petroleum Engineers

Men X, Tang CA, Wang S, Li Y, Yang T, Ma T (2013) Numerical simulation of hydraulic fracturing in heterogeneous rock: the effect of perforation angles and bedding plane on hydraulic fractures evolutions. In: ISRM international conference for effective and sustainable hydraulic fracturing, International Society for Rock Mechanics

Mills K, Jeffrey R, Karzulovic A, Alfaro M (2004) Remote high resolution stress change monitoring for hydraulic fractures. Proud to be miners, MassMin

Morrill J, Miskimins JL (2012) Optimization of hydraulic fracture spacing in unconventional shales. In: SPE hydraulic fracturing technology conference, Society of Petroleum Engineers

Nordgren R (1972) Propagation of a vertical hydraulic fracture. Soc Petrol Eng J 12(04):306–314

Olson J (2008) Multi-fracture propagation modeling: applications to hydraulic fracturing in shales and tight gas sands. In: The 42nd US rock mechanics symposium (USRMS), American Rock Mechanics Association

Perkins T, Kern L (1961) Widths of hydraulic fractures. J Petrol Technol 13(09):937–949

Puri R, King G, Palmer I (1991a) Damage to coal permeability during hydraulic fracturing. In: Low permeability reservoirs symposium, Society of Petroleum Engineers

Puri R, Yee D, Buxton TS, Majahan O (1991b) Method of increasing the permeability of a coal seam, Google Patents

Rafiee M, Soliman MY, Pirayesh E, Emami Meybodi H (2012) Geomechanical considerations in hydraulic fracturing designs. In: SPE Canadian unconventional resources conference, Society of Petroleum Engineers

Rogers S, Elmo D, Dershowitz W (2011) Understanding hydraulic fracture geometry and interactions in pre-conditioning through DFN and numerical modeling. In: 45th US rock mechanics/geomechanics symposium, American Rock Mechanics Association

Roussel NP, Sharma MM (2011a) Optimizing fracture spacing and sequencing in horizontal-well fracturing. SPE Prod Oper 26(02):173–184

Roussel NP, Sharma MM (2011b) Strategies to minimize frac spacing and stimulate natural fractures in horizontal completions. In: SPE annual technical conference and exhibition, Society of Petroleum Engineers

Roussel NP, Manchanda R, Sharma MM (2012) Implications of fracturing pressure data recorded during a horizontal completion on stage spacing design. In: SPE hydraulic fracturing technology conference, Society of Petroleum Engineers

Sepehri J (2014) Application of extended finite element method (XFEM) to simulate hydraulic fracture propagation from oriented perforations, Texas Tech University

Sepehri J, Soliman MY, Morse SM (2015) Application of extended finite element method to simulate hydraulic fracture propagation from oriented perforations. In: SPE hydraulic fracturing technology conference, Society of Petroleum Engineers

Siebrits E, Elbel J, Detournay E, Detournay-Piette C, Christianson M, Robinson B, Diyashev I (1998) Parameters affecting azimuth and length of a secondary fracture during a refracture treatment. In: SPE annual technical conference and exhibition, Society of Petroleum Engineers

Smith MB, Montgomery C (2015) Hydraulic fracturing. CRC Press, Boca Raton

Sneddon I (1946) The distribution of stress in the neighbourhood of a crack in an elastic solid. In: Proceedings of the Royal Society of London A: mathematical, physical and engineering sciences, The Royal Society

Tada H, Paris P, Irwin G (2000) The analysis of cracks handbook, vol 2. ASME Press, New York, p 1

Tang C (1997) Numerical simulation of progressive rock failure and associated seismicity. Int J Rock Mech Min Sci 34(2):249–261

Tang C, Yang W, Fu Y, Xu X (1998) A new approach to numerical method of modelling geological processes and rock engineering problems—continuum to discontinuum and linearity to nonlinearity. Eng Geol 49(3):207–214

Tang C, Tham L, Lee P, Yang T, Li L (2002) Coupled analysis of flow, stress and damage (FSD) in rock failure. Int J Rock Mech Min Sci 39(4):477–489

Tang C, Li L, Liang Z, Yang T, Tham L, Lee K, Tsui Y (2003) Numerical approach to influence of pore pressure magnitude and gradient on fracture propagation in brittle heterogeneous rocks. In: 10th ISRM congress, International Society for Rock Mechanics

Van As A, Jeffrey R (2000a) Caving induced by hydraulic fracturing at Northparkes mines. In: 4th North American rock mechanics symposium, American Rock Mechanics Association

van As A, Jeffrey R (2000b) Hydraulic fracturing as a cave inducement technique at Northparkes Mines. In: Proceedings, MassMin, pp 165–172

van As A, Jeffrey R (2002) Hydraulic fracture growth in naturally fractured rock: mine through mapping and analysis. In: Proceedings, 5th North American rock mechanics symposium and the 17th Tunnelling Association of Canada Conference. Toronto, ON

van As A, Jeffrey R, Chacon E, Barrera V (2004) Preconditioning by hydraulic fracturing for block caving in a moderately stressed naturally fractured orebody. Proc MassMin 2004:535–541

Wang S, Sun L, Au A, Yang T, Tang C (2009) 2D-numerical analysis of hydraulic fracturing in heterogeneous geo-materials. Constr Build Mater 23(6):2196–2206

Wang S, Sloan S, Fityus S, Griffiths D, Tang C (2013) Numerical modeling of pore pressure influence on fracture evolution in brittle heterogeneous rocks. Rock Mech Rock Eng 46(5):1165–1182

Weibull W (1951) A statistical distribution function of wide applicability. J Appl Mech 18:293–297

Weijers L, De Pater C (1992) Fracture reorientation in model cases. In: SPE formation damage control symposium, Society of Petroleum Engineers

Wright CA, Weijers L (2001) Hydraulic fracture reorientation: Does it occur? Does it matter? Lead Edge 20(10):1185–1189

Wu R, Kresse O, Weng X, Cohen C-E, Gu H (2012) Modeling of interaction of hydraulic fractures in complex fracture networks. In: SPE hydraulic fracturing technology conference, Society of Petroleum Engineers

Xu G, Wong S-W (2013) Interaction of multiple non-planar hydraulic fractures in horizontal wells. In: IPTC 2013: international petroleum technology conference

Yang TH, Li LC, Tham LG, Tang CA (2003) Numerical approach to hydraulic fracturing in heterogeneous and permeable rocks. In: Key Engineering Materials. Trans Tech Publications 243:351–356

Yang T, Tham L, Tang C, Liang Z, Tsui Y (2004) Influence of heterogeneity of mechanical properties on hydraulic fracturing in permeable rocks. Rock Mech Rock Eng 37(4):251–275

Zhai C, Li M, Sun C, Zhang J, Yang W, Li Q (2012) Guiding-controlling technology of coal seam hydraulic fracturing fractures extension. Int J Min Sci Technol 22(6):831–836